

## Estimating shear velocities in the oceanic crust from compliance measurements by two-dimensional finite difference modeling

Wayne C. Crawford, Spahr C. Webb, and John A. Hildebrand

Scripps Institution of Oceanography, University of California, San Diego, La Jolla

**Abstract.** The deep seafloor deforms under the pressure loading of linear ocean surface gravity (water) waves at low frequencies (0.003 to 0.04 Hz). The ratio of seafloor displacement to pressure loading as a function of frequency, known as the seafloor compliance function, depends on the shear velocity structure of the oceanic crust and upper mantle. Compliance measurements are used to estimate oceanic crustal structure, particularly within low shear velocity regions such as sediments, fractured rock, and partial melt. Compliance calculated from laterally homogeneous (one-dimensional, 1-D) crustal models shows that a buried low-velocity zone (LVZ) causes a peak in the compliance function at wavelengths 4 to 6 times longer than the LVZ depth, and that the compliance amplitude depends primarily on the LVZ shear velocity. A new numerical code allows forward modeling of compliance for two-dimensional oceanic crustal models. The new code demonstrates that the peak in the compliance function directly over a finite width LVZ reaches a maximum value at higher frequency, and is of smaller amplitude, than predicted from 1-D modeling. The compliance maximum persists outside of the region underlain by the LVZ but diminishes in amplitude and shifts to lower frequencies with increasing distance from the LVZ. The numerical models indicate that significant peaks in the compliance function indicate crustal LVZs, but that multiple compliance measurements are necessary to independently constrain the depth, location, and shear velocity of these features.

### 1. Introduction

We discuss a technique known as seafloor compliance inversion for determining the shear velocity structure of oceanic crust. The technique is particularly sensitive to regions of low shear velocity associated with magma and partial melt, or with high-porosity regions in the upper crust or in sediments. Melt plays a critical role in the creation of oceanic crust, while porosity plays an important role in the aging of young oceanic crust and affects sediment properties including stability and acoustic reflectivity. Crustal shear velocities are typically poorly constrained compared to other basic elastic parameters such as compressional velocity or density. The primary methods for estimating shear velocities in oceanic crust depend on active seismic sources, but these sources are generally inefficient at generating shear waves. In addition, low-velocity zones (LVZs) associated with melt or high porosity may trap seismic waves and attenuate seismic energy.

In seafloor compliance inversion, a shear modulus or shear velocity model is constructed based on the seafloor deformation under linear ocean surface gravity (water) waves. The technique was pioneered by *Yamamoto and Torii* [1986] using laterally homogeneous (one-dimensional, 1-D) seafloor

models to fit compliance measured in shallow water (less than 50 m). They refer to their instrumentation and data inversion package as the "bottom shear modulus profiler" [*Torii*, 1985; *Trevorrow et al.* 1988; *Yamamoto et al.*, 1989; *Trevorrow and Yamamoto*, 1991].

*Crawford et al.*, [1991] adapted this technique for work on the deep seafloor and modeled the seafloor compliance function over several 1-D crustal models, determining basic properties of the compliance function and introducing a linearized 1-D geophysical inverse method for calculating the smoothest crustal shear velocities consistent with measured compliance data. Shear velocity models constructed using this method and compliance measurements at several fast- and intermediate-rate oceanic spreading centers indicate the presence of mid-crustal LVZs inferred as regions of partial melt [*Crawford et al.*, 1991; *Crawford*, 1994]. These data are in good agreement with models derived from more conventional seismic techniques. The compliance data also image melt at the crust-mantle interface at 9°N on the East Pacific Rise axis [*Crawford et al.*, 1995]. Ridge crest compliance measurements show a rapid lateral variation in ocean spreading center structure compared to the ocean surface wavelengths generating the compliance signal. Fitting these compliance data using 1-D crustal models in such regions leads to interpretation errors; therefore we have developed a numerical code to calculate compliance over two-dimensional structures in the oceanic crust.

The numerical code uses a finite difference approximation to the equations of motion and applies the compliance

Copyright 1998 by the American Geophysical Union.

Paper number 97JB03532.  
0148-0227/98/97JB-03532\$09.00

boundary conditions. In this paper, we use the code to investigate the effect of laterally varying structure in two-dimensional (2-D) crustal models on the compliance function. Compliance functions are significantly modified by lateral variations in crustal elastic properties, although they retain the basic characteristics determined from 1-D modeling. The compliance function changes predictably based on changes in crustal structure, allowing estimation of laterally inhomogeneous crustal structure from seafloor compliance measurements.

We first define seafloor compliance and describe the compliance measurement procedure. We then estimate the relative sensitivity of the compliance function to compressional and shear velocities from the governing equations and use 1-D crustal models to determine the depth sensitivity of com-

pliance. The 2-D numerical code is next described and used to investigate the effect of lateral inhomogeneity on compliance by analyzing compliance functions calculated for simplified crustal models and a model East Pacific Rise cross section. Finally, we discuss how to interpret compliance measurements over laterally inhomogeneous oceanic crust.

## 2. Definition of Seafloor Compliance

Ocean surface gravity water waves generate pressure fluctuations that decay from the sea surface to the seafloor. Where significant pressure fluctuations from these waves reach the seafloor, the seafloor deforms measurably (Figure 1a). The amount of deformation depends on the pressure amplitude, the ocean surface wavelength  $\lambda_w$ , and the

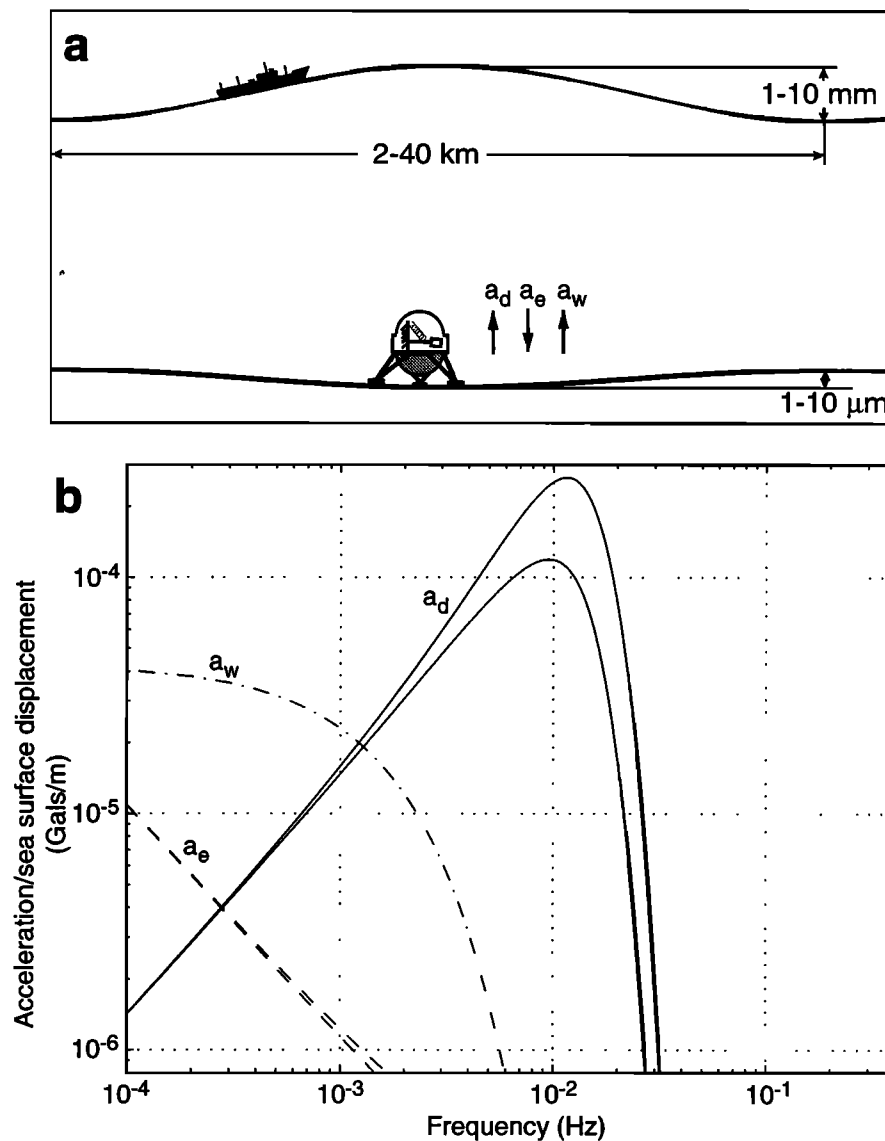


**Figure 1.** Harmonic acceleration sources on a seafloor seismometer:  $a_w$  is the gravitational attraction of the ocean surface wave,  $a_e$  is the gravitational attraction of the Earth, and  $a_d$  is the second time derivative of the seafloor displacement. The term  $a_d$  is needed to calculate seafloor compliance. (a) Cartoon of the ocean surface wave pressure source, seafloor displacement, and direction of accelerations acting on the seismometer. (b) Comparison of strength of different acceleration signal sources as a function of frequency;  $a_d$  dominates at frequencies above  $2 \times 10^{-3}$  Hz.

seafloor structure. Seafloor compliance is defined as the ratio of vertical seafloor displacement  $D_f(\omega)$  to the differential pressure at the seafloor  $P_{sf}(\omega)$ :

$$\xi(\omega) \equiv -D_f(\omega)/P_{sf}(\omega), \quad (1)$$

where  $\omega$  is angular frequency. The negative sign is necessary because positive pressure exerts a downward force on the seafloor, while displacement is positive upward. Seafloor compliance is measured in a frequency band for which the seafloor pressure and displacement signals are dominated by linear ocean surface gravity waves, so that the wavelengths and frequencies are related by the dispersion equation

$$\omega^2 = gk \tanh(k_w H), \quad (2)$$

where  $g$  is the local gravitational acceleration,  $H$  is the water depth, and  $k = 2\pi/\lambda_w$  is the ocean surface wavenumber [e.g., Gill, 1982, p.102]. The pressure signal amplitude at the seafloor is

$$P_{sf}(\omega) = \rho_w g h_w(\omega) / \cosh(k(\omega)H), \quad (3)$$

where  $\rho_w$  is the density of water and  $h_w(\omega)$  is the sea surface displacement. The  $\cosh(k(\omega)H)$  term strongly attenuates short wavelengths, so that the waves generate significant seafloor pressure fluctuations only for ocean surface wavelengths greater than the water depth.

The seafloor displacement under these waves depends on the crustal elastic structure and on the source pressure signal. For a given pressure signal, the displacement is larger over crust of lower shear modulus. The smallest seafloor displacements are therefore predicted for unsedimented deep ocean sites, because the pressure signal is smaller in the deep ocean than at near-shore sites, and the relatively high shear modulus of unsedimented oceanic crust (compared to sediments) allows only small displacements. One such unsedimented deep ocean site is the Juan de Fuca Ridge spreading axis, where the peak-to-peak amplitude of seafloor acceleration in the compliance frequency band is approximately 0.5  $\mu\text{Gal}$ , too small to be measured by typical ocean bottom seismometers. To detect this signal, we use a Lacoste-Romberg underwater gravimeter [Lacoste, 1967] as a low-frequency seismometer to measure seafloor acceleration. A differential pressure gauge [Cox *et al.*, 1984] is deployed with the gravimeter to measure seafloor pressure fluctuations.

Accelerations measured at the seafloor due to ocean surface waves have three sources: (1) the direct seafloor acceleration due to deformation ( $a_d$ ), (2) an acceleration caused by the change in the distance of the sensor from the Earth's center of mass due to the deformation ( $a_e$ ), and (3) an acceleration caused by the gravitational attraction of the ocean surface waves ( $a_w$ ). These accelerations are expressed as

$$a_d = -\omega^2 D_f, \quad (4)$$

$$a_e \approx \frac{2GM_E D_f}{r_e^3}, \quad (5)$$

$$a_w = 2\pi G \rho_w e^{-2\pi k H} h_w \quad (6)$$

where  $D_f$  is the seafloor displacement,  $r_e = 6.38 \times 10^6 \text{ m}$

is the mean radius of the Earth,  $G = 6.6732 \times 10^{-11} \text{ N m}^2 \text{ kg}^{-2}$  is the gravitational constant,  $M_E = 5.97 \times 10^{24} \text{ kg}$  is the mass of the Earth, and  $\rho_w \approx 1040 \text{ kg/m}^3$  is the water density.  $D_f$  is related to  $h_w$  using a combination of equations (1) and (3):

$$D_f = \frac{-\rho_w g h_w(\omega)}{\cosh(k(\omega)H)} \xi(\omega). \quad (7)$$

To express  $a_d$  and  $a_e$  in terms of  $h_w$ , substitute (7) into (4) and (5):

$$a_d \approx 9790 \omega^2 \frac{\xi(\omega)}{\cosh(k(\omega)H)} h_w, \quad (8)$$

$$a_e \approx -3.00 \times 10^{-2} \frac{\xi(\omega)}{\cosh(k(\omega)H)} h_w. \quad (9)$$

At seafloor depths between 2.2 and 2.7 km, compliance is measured in the frequency band between approximately 0.0035 and 0.03 Hz. In this range the deformation term,  $a_d$ , is dominant, but the gravitational attraction of the ocean surface waves,  $a_w$ , becomes significant at the lowest frequencies (Figure 1b). Before compliance is estimated using seafloor acceleration measurements, the  $a_w$  term must be removed from the acceleration signal. This is done using (3) and (6) to calculate  $a_w$  from the measured pressure signal.

Seafloor compliance is calculated from the acceleration and pressure spectra ( $\hat{S}_p(\omega)$  and  $\hat{S}_a(\omega)$ , respectively) using the equation

$$\hat{\xi}(\omega) = \frac{\hat{\gamma}_{pa}(\omega)}{\omega^2} \left( \frac{|\hat{S}_a(\omega)|}{|\hat{S}_p(\omega)|} \right)^{\frac{1}{2}} \quad (10)$$

where  $\hat{\gamma}_{pa}(\omega)$  is the coherence between the acceleration and pressure signals. Dividing by  $\omega^2$  in the equation converts the accelerations to displacements for harmonic forcing. The acceleration signal decreases and instrument noise increases with decreasing frequency, limiting measurement of seafloor accelerations to frequencies above approximately 0.0035 Hz at the deep seafloor (depths greater than 2 km). The compliance frequency band for deep ocean sites is therefore approximately 0.0035–0.03 Hz, corresponding to ocean surface wavelengths from 2 km to 40 km.

The coherence between the pressure and acceleration signals affects the compliance standard error and thus the accuracy of crustal models that can be constructed from compliance measurements [Crawford *et al.*, 1991]. In general, compliance measured at unsedimented deep ocean sites has larger standard errors than compliance measured at shallow sedimented sites due to the larger response of sediments to pressure loading. For example, measurements of seafloor pressure and acceleration on the unsedimented Juan de Fuca Ridge at approximately 2.2 km water depth have coherence of about 0.9 over most of the compliance frequency band (Figure 2b), resulting in 1–15% standard errors (Figure 2c). For comparison, compliance measurements on a thickly sedimented California coastal site (0.4–0.8 km water depth) have standard errors from 0.3 to 1% (Figure 3c).

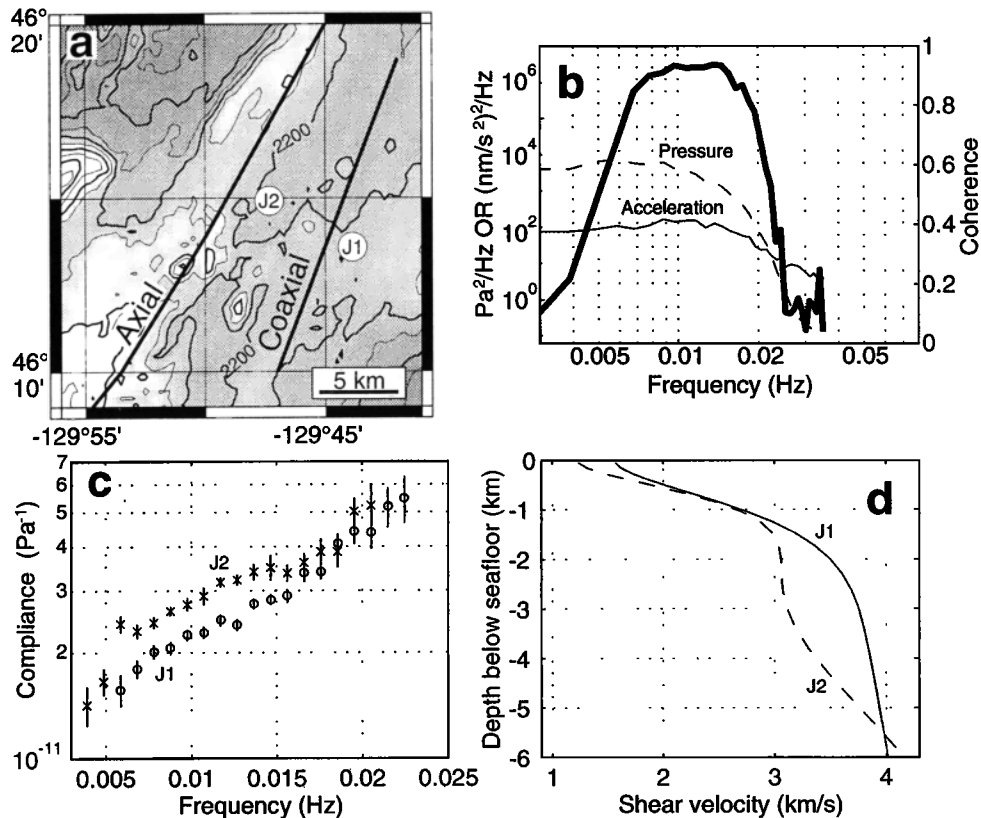


**Figure 2.** Compliance measurements from the intermediate spreading Juan de Fuca Ridge. (a) Site location map. The approximate location of neovolcanic zones associated with the Axial Volcano north rift zone and the Coaxial segment spreading axis are plotted as thick lines. (b) Pressure and acceleration spectra (thin lines) and coherence (thick line) from site J2. (c) Compliance and standard errors estimated at the two sites. (d) Minimum structure 1-D shear velocity models fitting the compliance data.

### 3. Compliance Properties

The seafloor compliance function is sensitive to variations in crustal shear velocity with depth, and in particular to regions of low shear velocity. In this section, we present examples of compliance measurements and relate their major features to crustal shear velocity variations. Compliance is most directly dependent on shear modulus,  $\mu$ , rather than on shear velocity  $V_S = \sqrt{\mu/\rho}$ . However, it is generally more convenient to use shear velocity models because oceanic crustal models are usually presented in terms of seismic velocities. Seafloor pressure fluctuation spectra, acceleration spectra, coherences and compliances have been measured at an oceanic spreading center (Figure 2) and over sediments near a fault through continental borderlands (Figure 3). Compliance measured at these two locales can be fit using 1-D seafloor models, although the compliance functions change over distances short compared to the forcing ocean surface wavelength. These measured compliance functions motivate investigation of the effect of vertical shear velocity variations on the compliance function. Later we examine how lateral variations in crustal structure affect both the compliance function and the interpretation of crustal structure from compliance measurements.

The first example compliance measurements lie across the intermediate-spreading-rate Juan de Fuca Ridge at 46°12'–

20'N (Figure 2). The measurement sites are just north of Axial Volcano, a large seamount that marks the intersection of the Juan de Fuca Ridge with the Cobb-Eickelberg seamount chain. Two neovolcanic zones overlap here, one traveling along the northern rift zone of Axial Volcano, and the other (the so-called Coaxial neovolcanic zone) bisecting an apparent rift valley to the east. The Coaxial neovolcanic zone is a more typical spreading center morphology. The water depth is 2.4–2.6 km and compliance values were obtained between 0.004 and 0.0225 Hz, corresponding to forcing ocean surface wavelengths from 3 to 38 km. The two compliance measurement sites are separated by 5.5 km on a line perpendicular to the neovolcanic zones. Compliance function amplitudes at the two sites are approximately the same at the highest and lowest frequencies, but compliance at intermediate frequencies is significantly higher at the site nearest to the Axial Volcano northern rift zone. We will show below that the higher compliance at intermediate frequencies indicates a low shear velocity zone within the crust.

A second pair of compliance measurements (Figure 3) are from the Newport-Inglewood-Rose Canyon fault zone, a 240 km long, 0.4–4 km wide zone of strike-slip faults that extends from the Los Angeles Basin to downtown San Diego and possibly south into Mexico [Fischer and Mills, 1991]. The fault zone lies offshore in water depths up to 1 km between La Jolla and Newport Beach, California. Cold water

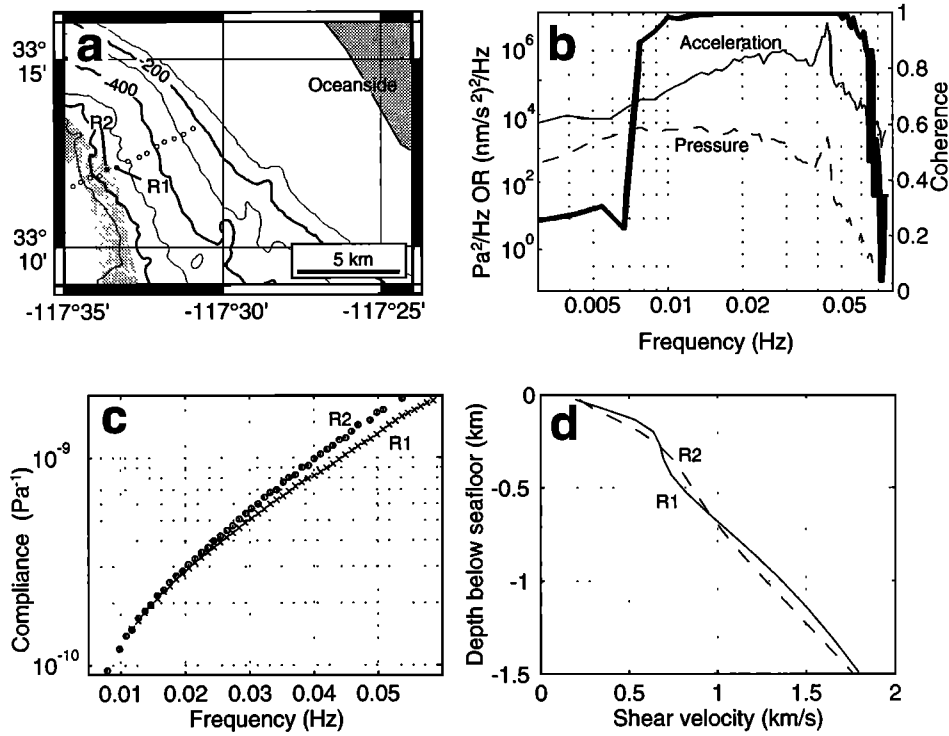


**Figure 3.** Compliance measurements across the Newport-Inglewood fault zone in the California continental borderlands. (a) Site location map. The fault zone is indicated by the shaded area in the southwest map corner. Compliance measurement sites are indicated by circles; the two compliance measurements shown are from the sites indicated by solid circles. (b) Pressure and acceleration spectra (thin lines) and coherence (thick line) from site R2. (c) Compliance and standard errors estimated at the two sites. The error bars, visible inside the circles, are too small to be seen behind the crosses. (d) Minimum structure 1-D shear velocity models fitting the compliance data.

seeps are located at various points along the fault zone (P. Lonsdale, personal communication, 1997). A line of compliance measurements across the fault zone at  $33^{\circ}12'N$  was designed to investigate changes in shear modulus caused by pore water expulsion associated with the fault. We show compliance from two sites separated by 750 m at the eastern edge of the fault zone at  $33^{\circ}12'N$ . The water depth is approximately 530 m and compliance values were obtained between 0.008 and 0.057 Hz, corresponding to forcing wavelengths between 0.5 and 9 km. Compliance functions measured at the two sites are similar at low frequencies, but compliance is higher at the further offshore site for frequencies above 0.025 Hz. We will show below that this indicates the seaward site overlies lower shallow shear velocities than the shoreward site.

### 3.1. Compliance Sensitivity to Elastic Parameters

To determine the effect of crustal elastic properties on seafloor compliance in the simplest case, we consider first the compliance function sensitivity to elastic parameters in a uniform half-space. *Sorrels and Goforth [1973]* derived the equation for compliance over a homogeneous, isotropic half-space under quasi-static forcing:

$$\xi(\omega) = \frac{\lambda + 2\mu}{k(\omega)2\mu(\lambda + \mu)}, \quad (11)$$

where  $\mu$  and  $\lambda$  are Lamé parameters related to the compres-

sional velocity,  $V_P$ , and the shear velocity,  $V_S$ , by the equations

$$V_P \equiv \sqrt{(\lambda + 2\mu)/\rho} \quad (12)$$

and

$$V_S \equiv \sqrt{\mu/\rho}. \quad (13)$$

The quasi-static assumption made in the derivation of (11) is valid as long as velocities in the half-space are much greater than the ocean surface gravity wave phase speed. Equation (11) shows that compliance of the half-space is independent of the material density,  $\rho$ . If compliance is normalized by multiplying by the wavenumber,  $k(\omega)$ , it is also independent of frequency. For the remainder of this paper, any reference to compliance will mean compliance normalized by the wavenumber:

$$\eta(\omega) = k(\omega)\xi(\omega). \quad (14)$$

The relative importance of  $\mu$  (also known as the shear modulus or rigidity) and  $\lambda$  is illustrated by defining

$$a \equiv \frac{\lambda + 2\mu}{2(\lambda + \mu)}. \quad (15)$$

Equations (11), (14), and (15) then give

$$\eta(\omega) = \frac{a}{\mu}. \quad (16)$$

The value of  $a$  depends only weakly on the Lamé parameters in oceanic crust and mantle, ranging from 0.5 for melt and poorly consolidated sediments ( $\mu \rightarrow 0$ ) to 0.75 for deep crustal and upper mantle rocks ( $\mu \approx \lambda$ ). By choosing  $a = 0.625$ ,  $1/\mu$  can be determined to within 20% from the compliance with no knowledge of  $\lambda$ . The accuracy is improved by using experimentally determined relationships between  $\mu$  and  $\lambda$ , or by constraining  $\mu$  with a pre-existing estimate of  $\lambda$ . Compliance is at least 5 times more sensitive to changes in  $\mu$  than to changes in  $\lambda$  [Crawford *et al.*, 1991], so uncertainties in  $\lambda$  map to much smaller errors in  $\mu$ .

The Lamé parameter  $\lambda$  is rarely constrained in oceanic crust. Instead, seismic refraction and reflection studies often provide a compressional velocity estimate. Because the compressional velocity depends on the shear modulus, compliance is more sensitive to compressional velocity variations than to changes in  $\lambda$ . We use partial derivatives to estimate this sensitivity, combining (11), (12), (13), and (14) to obtain

$$\eta = \frac{V_P^2}{2V_S^2(V_P^2 - V_S^2)}. \quad (17)$$

Using this equation, shear velocity is more convenient for comparison with compressional velocity than is the shear modulus. The partial derivatives of compliance in a half-space with respect to compressional and shear velocities are

$$\frac{\partial \eta}{\partial V_P} = \frac{-V_P}{(V_P^2 - V_S^2)^2} \quad (18a)$$

$$\frac{\partial \eta}{\partial V_S} = \frac{-V_P^2 [V_P^2 - 2V_S^2]}{V_S^3 (V_P^2 - V_S^2)^2}. \quad (18b)$$

The ratio  $R$  of the partial derivatives, normalized by the seismic velocities, gives an estimate of the relative sensitivity of compliance to these seismic velocities,

$$R = \frac{V_S}{V_P} \frac{\partial \eta / \partial V_S}{\partial \eta / \partial V_P} = (V_P^2 / V_S^2 - 2) \quad (19)$$

For  $R = 1$ , the compliance function is equally sensitive to compressional and shear velocities; for  $R > 1$ , the compliance function is most sensitive to changes in shear velocity. In oceanic crust,  $V_P^2 / V_S^2$  ranges from 3 for a Poisson solid to infinity for melt, so  $R$  ranges from 1 to infinity. Because compliance is insensitive to compressional velocity for  $R$  much greater than 1, shear velocity values determined from compliance measurements are independent of the compressional velocity estimate in areas of high  $V_P^2 / V_S^2$  such as poorly consolidated sediments and regions of partial melt. Where the crust is solid and unfractured, as in crustal gabbros ( $V_P^2 / V_S^2 = 3.57\text{--}3.65$  [Christensen, 1978; Spudich and Orcutt, 1980]), and mantle peridotites ( $V_P^2 / V_S^2 = 3.00\text{--}3.20$  [Christensen, 1978; Horen *et al.*, 1996]), the accuracy of the shear velocity model depends on the accuracy of the compressional velocity model.

### 3.2. Compliance Sensitivity to Crustal Structure as a Function of Depth

Measurements of seafloor compliance are useful for determining crustal structure because variations in the com-

pliance function with frequency are related to variations in elastic parameters with depth. As was the case with the half-space model, crustal density and the forcing wave frequency have no effect on the compliance function for nonuniform crust (see the appendix), except that the ocean wave frequency determines the wavelength causing the deformation. A velocity anomaly in the crust has the strongest effect on the compliance function at frequencies corresponding to ocean surface wavelengths between 4.2 and 6.2 times the anomaly depth. We demonstrate this below using 1-D models.

To show the relationship between pressure wavelength and the depth of shear velocity anomalies in oceanic crust, we calculate seafloor compliance over 1-D models consisting of a low-velocity layer sandwiched between two higher-velocity layers (Figure 4). The compliance function for these models is calculated using a modification of the propagator matrix method [Aki and Richards, 1980] that increases numerical stability by propagating minor vectors rather than displacements and stresses [Gomberg and Masters, 1988]. For a given ratio of the LVZ shear velocity to the shear velocity in the surrounding rock, the forcing pressure wavelength at the compliance function maximum,  $\lambda_{w,peak}$ , is proportional to the LVZ depth,  $d_{LVZ}$ . The constant of proportionality varies with the shear velocity in the LVZ, ranging from 4.2 for a weak anomaly (LVZ shear velocity = 90% of the surrounding shear velocity) to 6.2 for a strong anomaly (LVZ shear velocity = 0.1% of the surrounding shear velocity). These values may be used to estimate the maximum depth constrained by a compliance measurement, based on the longest ocean surface wavelengths for which significant coherence exists between seafloor pressure and acceleration. The Juan de Fuca compliance functions presented earlier have a maximum ocean surface wavelength of approximately 38 km, so crustal structure there is constrained to depths of at least  $38/6.2 = 6.1$  km. Similarly, the California continental borderlands crustal structure is constrained to at least 1.5 km beneath the seafloor.

### 3.3. One-Dimensional Shear Velocity Models Constructed Using Compliance Inversion

Figures 2d and 3d show “minimum structure” 1-D shear velocity models fitting compliance measured at the Juan de Fuca Ridge and at the Newport-Inglewood-Rose Canyon fault zone. The crustal models agree with the two compliance properties described above: (1) an increase in compliance amplitude indicates a decrease in shear velocity within the crust, and (2) compliance function variations with frequency are related to shear velocity variations with depth, with lower frequencies sensing deeper structure. The shear velocity model is constructed using a linearized geophysical inversion technique called Occam’s inversion [Constable *et al.*, 1987], described by Crawford *et al.* [1991]. Using a starting model for compressional velocity and shear velocity, the program adjusts the shear velocity profile to fit the compliance data within the measurement errors. The program finds the smoothest possible shear velocity profile (in the sense of the smallest root mean square second difference),

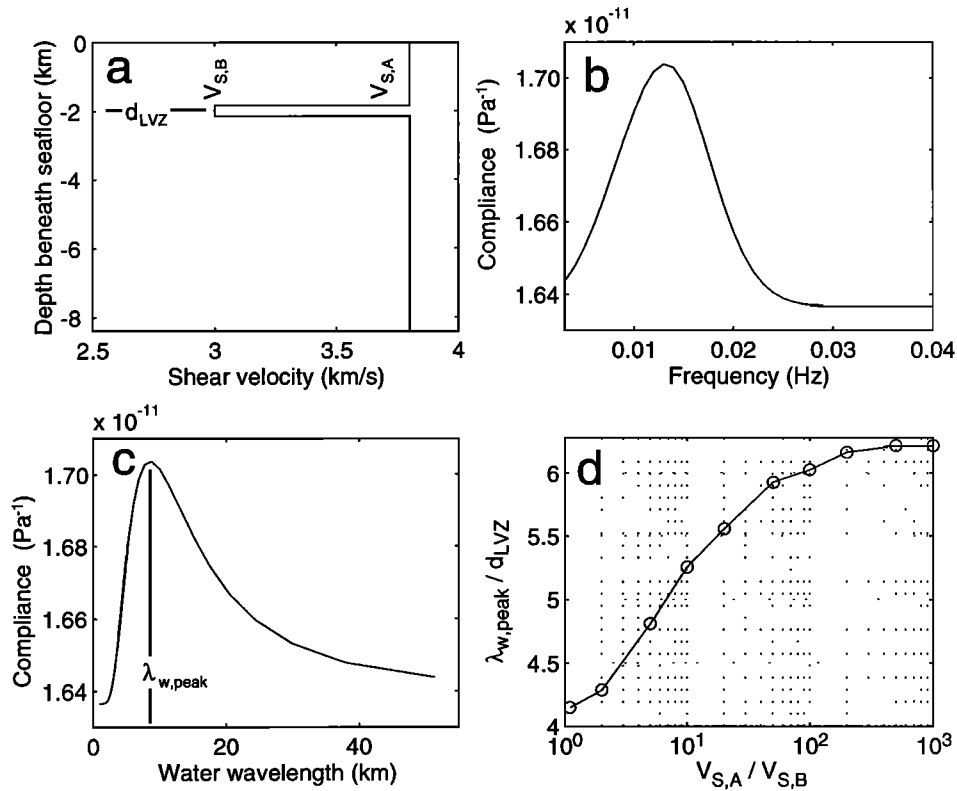


**Figure 4.** Relationship between LVZ depth and the water wavelength at which the compliance function is maximum. Compliance of a sample LVZ model is also plotted versus both frequency and forcing water wavelength, because compliance is measured (and typically displayed) as a function of frequency, but its sensitivity to crustal structure is entirely a function of the forcing water wavelength. (a) Sample shear velocity profile, with  $d_{LVZ}$  the LVZ depth,  $V_{S,A}$  the bulk shear velocity, and  $V_{S,B}$  the shear velocity in the LVZ. (b) Compliance as a function of frequency for the sample model beneath a 2.5 km deep ocean. The peak in compliance is created by the LVZ. (c) Compliance as a function of the forcing ocean surface wavelength, with the wavelength at the peak in the compliance function designated  $\lambda_{w,peak}$ . (d) The ratio of the peak wavelength to LVZ depth plotted versus the velocity anomaly amplitude ( $V_{S,A}/V_{S,B}$ ).

putting large excursions in the shear velocity profile only if required by the data.

The compressional velocity model used in the Juan de Fuca Ridge compliance data inversions comes from a seismic refraction study of the Northern Symmetrical segment by *Christeson et al.* [1993]. The shear velocity profiles determined from the compliance data are similar to one another in the upper 2 km of crust and at depths greater than 5 km beneath the seafloor (Figure 2d). Between 2 and 5 km beneath the seafloor, site J2 has anomalously low shear velocities. The low shear velocities may indicate a small percentage of partial melt beneath site J2, or (as we show later) may be caused by a larger LVZ adjacent to site J2. Only a series of measurements at adjacent sites can differentiate between these two possibilities.

The two compliance-based shear velocity models from the Newport-Inglewood-Rose Canyon fault zone differ significantly in the upper 0.7 km of sediment (Figure 3d). Differences between deeper velocities have no significant effect on the compliance signal. The compressional velocity model used in the compliance data inversions was derived from seismic reflection and refraction analyses of the California continental borderlands by *Teng and Gorline* [1989]. Shear

velocities in the 1-D model beneath site R1, on the landward side of the fault zone, increase rapidly in the first 0.2 km beneath from the seafloor. The velocity gradient beneath site R1 decreases between 0.2 and 0.5 km beneath the seafloor, before increasing to match the velocities at site R2 below 0.65 km. The shear velocity gradient beneath site R2 gradually decreases with increasing depth. Lower shear velocities in the uppermost 250 m at site R2 generate the higher compliance observed above 0.025 Hz. The change in shallow sediment shear velocities across the eastern edge of this fault zone indicates that the faulting affects the sediment properties.

#### 4. Two-Dimensional Modeling

The 1-D shear velocity models shown above indicate that crustal structure varies laterally at both the Juan de Fuca Ridge and across the Newport-Inglewood-Rose Canyon fault zone. In both locales, the ocean surface wavelengths causing the deformation are significantly longer than the distance between measurement sites. The shear velocity structure determined using 1-D modeling is therefore a smoothed representation of the actual crustal structure. In addition, lateral vari-

ation in structure may affect the amplitude and frequency of compliance function features, so that shear velocity models based on 1-D compliance calculations may incorrectly estimate both the depth and intensity of shear velocity anomalies. For this reason, we have developed a numerical code to calculate the compliance function over two-dimensional (2-D) models.

#### 4.1. Finite Difference Code

The numerical code uses a finite difference approximation in two dimensions to the equations of motion in an elastic solid with the appropriate compliance boundary conditions (see the appendix). The code assumes a harmonic excitation by the source waves and a laterally periodic model. The periodic boundary condition requires the wavelengths to be an integral divisor of the model width. The code also requires zero motion at the bottom boundary. Test runs indicate that the solution is not damped by the fixed bottom boundary for ocean surface wavelengths less than or equal to the depth to the bottom boundary. Most of our models are 60 km wide by 30 km deep, so the maximum wavelength for which compliance is calculated is 30 km. The minimum grid spacing used for the 60 km by 30 km models is 100 m. Stability concerns require the structure and the forcing pressure signal to vary only on wavelengths longer than 10 grid elements [Aki and Richards, 1980], so the minimum wavelength for which compliance is calculated is 1 km. In the 2-D models, discrete areas of constant elastic parameters are connected by a smooth transition zone 12 to 15 elements across. The smoothing is applied to  $1/\mu$  and  $1/\lambda$ , rather than  $\mu$  and  $\lambda$ , because test runs indicate that this smoothing gives the most accurate 2-D compliance.

The centered finite difference approximation to the gradient of a function (in this case, the compliance function) for a grid size of  $h$  meters has  $O(h^2)$  error [Aki and Richards, 1980]. This error can be reduced by assuming that the compliance calculated at each seafloor point for a given model is the true compliance, plus an error proportional to  $h^2$ :

$$\eta_h = \eta + Eh^2 + \text{higher order terms.} \quad (20)$$

The  $h^2$  error term is eliminated by calculating compliance for two models with identical elastic properties but different grid spacings,  $h_a$  and  $h_b$ . Equation(20) is then manipulated to obtain

$$\eta = \frac{\eta_{h_a} h_b^2 - \eta_{h_b} h_a^2}{h_b^2 - h_a^2} + \text{higher order terms.} \quad (21)$$

We refer to this method of removing the  $O(h^2)$  error as quadrature error correction.

#### 4.2. Calibration of 2-D Code

We calibrate the 2-D code by calculating compliance for simple models for which a reference compliance can be determined using established techniques. The compliance function calculated using the 2-D code is compared to a reference function. The principal error source in the finite dif-

ference approximation is the discretization of the model and derivatives.

To investigate the effect of the shear modulus or shear velocity on modeling accuracy, we use the finite difference code to calculate the compliance function over two half-space models. One model has elastic parameters similar to those found in oceanic crustal gabbros ( $V_P = 7$  km/s,  $V_S = 3.8$  km/s,  $\rho = 3000$  kg/m<sup>3</sup>,  $\mu = 43$  GPa), while the other has lower elastic parameter values, consistent with porous upper crust, crust with a small percentage of partial melt, or highly consolidated sediments ( $V_P = 5$  km/s,  $V_S = 1.5$  km/s,  $\rho = 2500$  kg/m<sup>3</sup>,  $\mu = 5.6$  GPa). The calculated compliance functions are compared to those found using (11) for a half-space. For the gabbroic rock model, compliance calculated in the frequency range from 0.008 Hz to 0.031 Hz, using quadrature error correction for models with 100- and 125-m grid spacing, results in a model error ranging from 0.004% at the lowest frequency to 0.5% at the highest frequency. The calculated compliance is always less than the reference value, and the error amplitude increases monotonically with increasing frequency (decreasing ocean surface wavelength) because the grid size is a larger fraction of the shorter wavelengths. For the model with lower shear modulus (velocity), error amplitudes range from 0.4% to 5%. Again, the calculated compliance is less than the reference value, and the error increases monotonically with increasing frequency.

A second test uses a laterally homogeneous crustal model containing a 1000 m thick LVZ centered 3 km beneath the seafloor (Figure 5a). Compliance calculated using the finite difference code is compared with compliance calculated using the 1-D minor vector propagator matrix code. The model has typical lower crustal properties ( $V_P = 7$  km/s,  $V_S = 3.8$  km/s,  $\rho = 3000$  kg/m<sup>3</sup>, and  $\mu = 43$  GPa) for depths outside

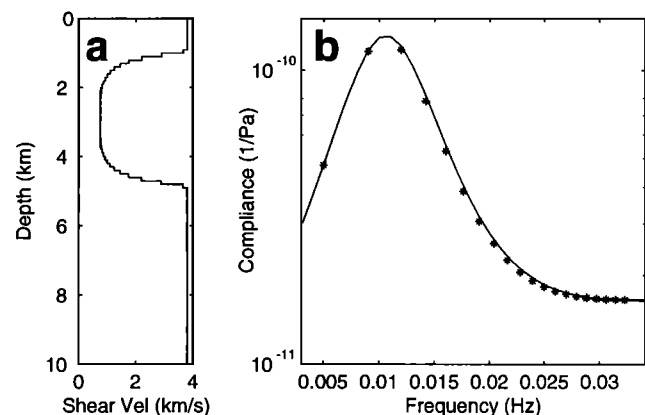


**Figure 5.** Laterally homogeneous model with an LVZ centered 3 km beneath the seafloor. (a) Model shear velocities (minimum  $\mu = 1.4$  GPa). The LVZ appears thicker than 1 km in the shear velocity profile because the sine taper between the LVZ and surrounding elastic values is applied to  $1/\mu$  rather than the shear velocity, and, at low shear velocities, a large change in  $1/\mu$  corresponds to a small change in shear velocity. (b) Compliance estimated using the minor vector method of *Gomberg and Masters* [1988] (solid line) and the 2-D finite difference algorithm (asterisks).

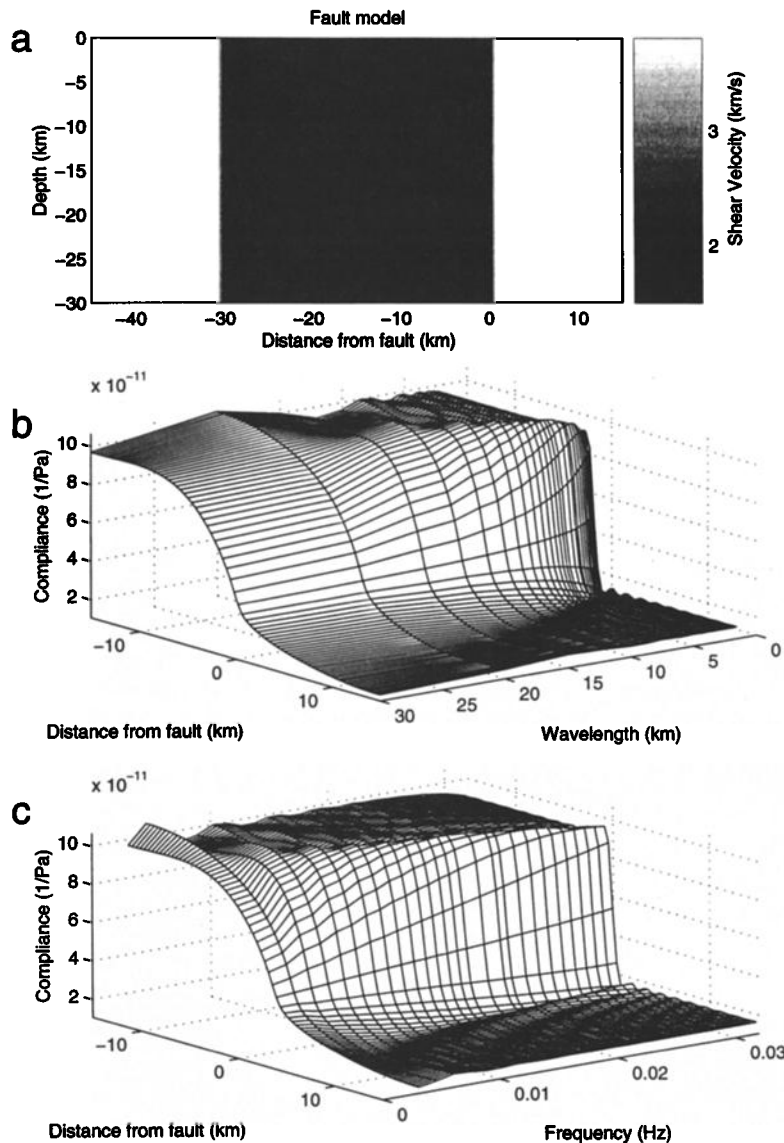


**Figure 6.** Fault model, consisting of two homogeneous bodies connected at a vertical interface. The model is laterally periodic. Because compliance values are symmetric about the -15 km locations, compliance values are shown for only one-half the model. (a) Model shear velocities. (b) Seafloor compliance as a function of forcing wavelength and lateral distance. (c) Seafloor compliance as a function of frequency and lateral distance.

of the LVZ, with a 1500 m thick transition to the LVZ properties ( $V_P = 4$  km/s,  $V_S = 0.75$  km/s,  $\rho = 2500$  kg/m<sup>3</sup>). The compliance function calculated using the finite difference code fits the reference compliance to within 1%. Both the 1-D and 2-D compliance signals have peaks near 0.01 Hz associated with the LVZ and agree well on the amplitude and frequency for the signal peak.

## 5. Compliance Function for 2-D Models

To determine the effect of laterally varying structure on the compliance function, we calculated 2-D compliance functions for models of (1) a simple vertical “fault”, (2) finite width LVZs, and (3) a cross section of a fast spreading oceanic spreading center.

The 1-D minor vector method of calculating seafloor compliance is inappropriate for these models. Throughout this

section, however, we calculate compliance functions using the 1-D code to compare with the 2-D results. For the remainder of this paper, when we refer to the “1-D approximation” of compliance over a 2-D model, we mean compliance functions calculated using the minor vector method at each model surface element by assuming the elastic parameters directly beneath the site have infinite horizontal extent. The 1-D approximation is, by definition, insensitive to crustal structure to the side of a given seafloor measurement site.

### 5.1. Vertical Fault

The fault model (Figure 6a) demonstrates the lateral sensitivity of the compliance function to varying crustal structure in the simplest possible model. The model consists of two homogeneous blocks placed beside each other, one block

having elastic parameters similar to gabbroic crust ( $V_P = 7$  km/s,  $V_S = 3.8$  km/s,  $\rho = 3000$  kg/m<sup>3</sup>,  $\mu = 43$  GPa), the other block having elastic parameters similar to consolidated sediments ( $V_P = 5$  km/s,  $V_S = 1.5$  km/s,  $\rho = 2500$  kg/m<sup>3</sup>,  $\mu = 5.6$  GPa). The elastic parameters do not change with depth. The “fault” is a 1500 m wide sine taper of elastic parameters between the two blocks. Because the model is laterally periodic, elastic parameters are the same at the left and right model edges, requiring two faults in the model. For this and all subsequent models, compliance functions shown are quadrature error corrected. To set up this correction, compliance is also calculated for two 60 km wide by 30 km deep models, one with 100 m grid spacing and the other with 125 m grid spacing. For the fault model only, compliance is calculated over a third model, 20 km wide by 10 km deep with 50 m grid spacing. Compliance calculated using this model is combined with compliance calculated using the 100 m grid model to obtain a second quadrature-error-corrected compliance. This compliance estimate is used to investigate the effect of grid size on compliance function error.

Compliance shown in Figures 6b (for wavelength) and 6c (for frequency) is calculated from the 100 and 125 m grid size models. As is expected, compliance over the low-shear-velocity block is higher than compliance over the high-shear-velocity block. Toward the center of each block, compliance approaches the 1-D values. Nearing the fault, the transition between the end-member compliance values is smoothest for the longest forcing wavelengths (lowest frequencies).

There are “ripples” in the compliance function (Figures 6b and 6c) that are mostly associated with the numerical error due to the finite grid size, despite quadrature correction. To demonstrate this, (Figure 7 compares quadrature-error-corrected compliance for a 1.5 km ocean surface wavelength based on using the 100 and 125 m grid size models (large-grid compliance), and the 50 and 100 m grid size models (small-grid compliance). The small-grid compliance function is smoother and fits the 1-D compliance values away from the fault zone better than the large-grid compliance function. The large-grid compliance function oscillates near the fault and is too low over the low-velocity block. The underestimate of compliance over the low-shear-velocity block is as expected from the numerical errors seen in the half-space models at high frequencies. The oscillations are caused by misalignment of numerical ringing in the 100 m and 125 m grid models. Comparisons show that compliance calculated for ocean surface wavelengths shorter than 4 km is better estimated using the small-grid models. However, the memory and cost limitations do not allow calculation of 50 m grid size compliance for a range of frequencies equivalent to those measured at the seafloor. Because the small-grid compliance cannot be used to evaluate real measurements, we show only large-grid compliance in Figure 6 and from here forward. It should be noted, however, that spatial oscillations in compliance for short-wavelength forcing are artifacts of the numerical approximation.

The lateral distance required for compliance values to rise from the 1-D values of the “hard rock” block to the 1-D val-

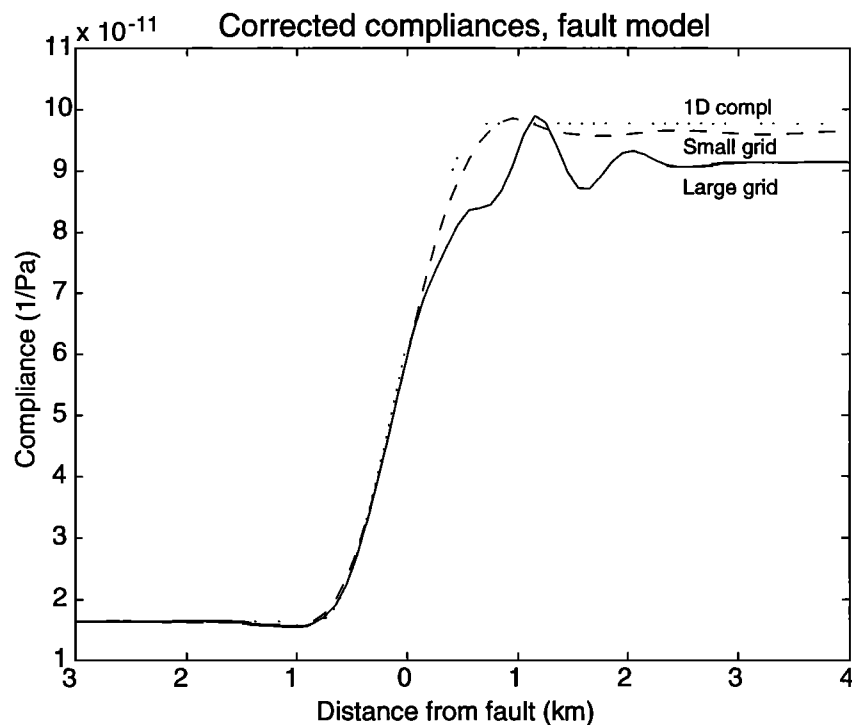


**Figure 7.** Seafloor compliance plotted as a function of distance from the fault for 1.5 km wavelength ocean wave forcing, using (1) compliance calculated from 100 and 125 m grid models (solid line), (2) compliance calculated from 100 and 50 m grid models (dashed line), and (3) 1-D compliance (dotted line).

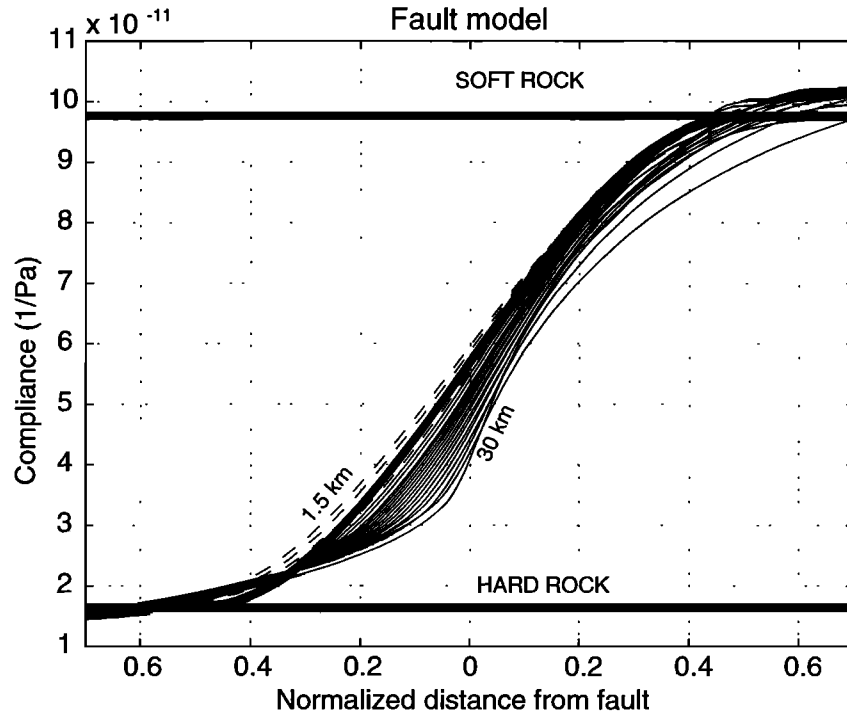


**Figure 8.** Compliance across the fault, normalized by dividing by  $(\lambda_w + 1.5 \text{ km})/2$ . Thin solid lines are compliance functions calculated for modeled ocean surface wavelengths greater than 4 km, using the large 100 and 125 m grid models. Thin dashed lines are compliance functions calculated for modeled ocean surface wavelengths less than 4 km, using the 100 m and 50 m grid models. Thick straight lines represent 1-D compliance of the “hard rock” and “soft rock” blocks used in the model. Thick curved line is one half cycle of a sine wave with wavelength 2.

ues of the “soft rock” block gives an estimate of the compliance function lateral sensitivity. This distance is well fit by the straight line  $d = (1.5 \text{ km} + \lambda_w)/2$ , where  $\lambda_w$  is the ocean surface wavelength and 1.5 km is the width of the fault transition zone. The factor of 2 arises because the distance required for compliance to rise to a new value is one-half the response “wavelength”. Figure 8 shows compliance as a function of distance across the fault, normalized by  $d$ . For comparison, one-half of a sine wave of normalized wavelength 2 is also plotted. Although the compliance values change from soft rock to hard rock values over approximately the same normalized distance, the shape of the transition changes systematically with changes in forcing wavelength. At the longest forcing wavelengths, compliance changes much more rapidly on the soft rock side of the fault than on the hard rock side. In addition, the transition between low and high compliance values is shifted to the soft rock side of the fault. In other words, long-wavelength (low frequency) compliance on the soft rock side of the fault is more strongly affected by the neighboring hard rock than vice versa. It appears that the lateral rate of change of the compliance function over laterally varying structure is affected by the material shear strength. Intuitively, the greater rigidity of the hard rock block makes it more resistant to the motion of the soft rock block than vice versa.

## 5.2. Low-Velocity Zones

One of the most important properties of the seafloor compliance function is its sensitivity to LVZs associated with

partial melt in oceanic crust. A crustal LVZ may be detected with a single compliance measurement, but the size and shear velocity of the feature can only be constrained if the effect of finite LVZ width is understood. We calculate here the compliance function over two models containing finite width LVZs. The LVZ in the first model is centered 3 km beneath the seafloor (Figure 9a), and the LVZ in the second model is centered 6 km beneath the seafloor (Figure 10a). In both models, the LVZ is 3000 m wide by 1000 m deep, with a 1500 m transition on all sides to the elastic parameters of the surrounding gabbroic material.

Figures 9 and 10 show seafloor compliance calculated for the LVZ models using the finite difference code. Both models generate a peak in the compliance function that is spatially centered over the LVZ. The compliance maximum is located at higher frequency (shorter wavelength) over the 3 km deep LVZ than over the 6 km deep LVZ, as predicted from 1-D modeling. The compliance function peak amplitude is also larger over the 3 km deep LVZ than over the 6 km deep LVZ. The decreasing compliance sensitivity to structure with increasing depth is consistent with the results of 1-D modeling. However, the spatial extent and the amplitude versus frequency characteristics of the compliance peak over the LVZ are different from those predicted using the 1-D approximation.

Figure 11 compares compliance functions over the LVZs to those predicted on axis using the 1-D approximation. For both models, the on-axis (0 km, in the figure) compliance peak is centered at higher frequency and is of smaller am-

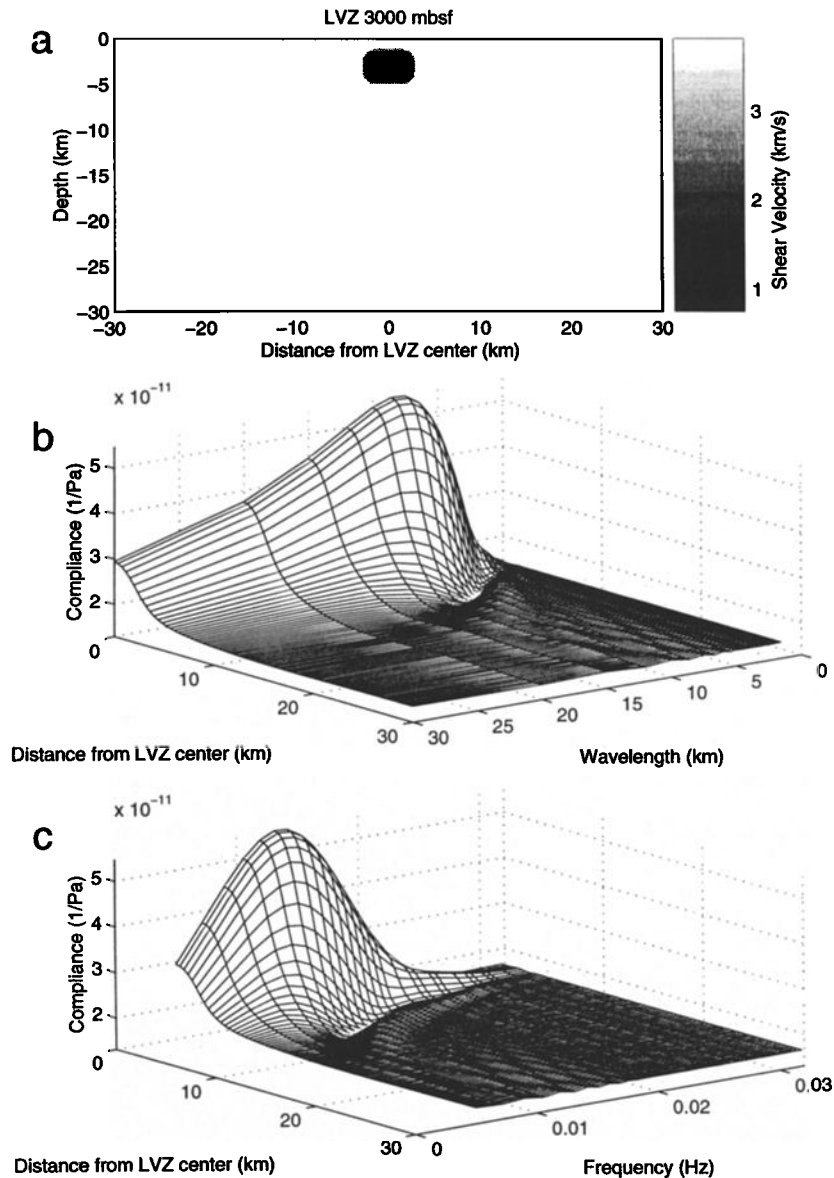


**Figure 9.** LVZ centered 3 km below the seafloor.  $V_P = 4$  km/s,  $V_S = 0.75$  km/s,  $\rho = 2500$  kg/m<sup>3</sup>, and  $\mu = 1.4$  GPa in the LVZ, while the surrounding material is uniform gabbroic rock ( $V_P = 7$  km/s,  $V_S = 3.8$  km/s,  $\rho = 3000$  kg/m<sup>3</sup>,  $\mu = 43$  GPa). Because compliance values are symmetric about the origin, compliance values are shown for only one-half the model. (a) Shear velocity. (b) Seafloor compliance as a function of forcing wavelength and horizontal distance from the center of the model. (c) Seafloor compliance as a function of frequency and horizontal distance.

plitude than the peak predicted using the 1-D approximation. As compliance measurements shift off axis, the peak in compliance decreases in amplitude and shifts to lower frequencies. These properties are explained by the wavelength-dependent spatial smoothing of the underlying structure. At low frequencies, the compliance signal is generated by long-wavelength ocean waves which average crustal structure over larger lateral area than do the shorter ocean surface wavelengths at higher frequencies. Over the LVZ, compliance is more strongly damped by structure to the side of the LVZ at low frequencies than at high frequencies. This results in a shift in the compliance peak to higher frequencies in the 2-D model than in a 1-D model. To the side of the LVZ, compliance at high frequencies decreases much more rapidly

than at low frequencies, resulting in an off-axis shift in the compliance peak to lower frequencies. One-dimensional compliance modeling can only match these changes in peak frequency by changing the LVZ depth. A 1-D shear velocity model generated from the on-axis compliance data would show a sub-crustal LVZ that is too shallow and has shear velocities that are too high. Because the compliance peak shifts to lower frequencies with increasing distance from the LVZ, 1-D shear velocity models constructed from the off-axis compliance would show the LVZ depth increasing away from the LVZ center.

Because 2-D compliance can be explained, to first order, as a smoothed version of 1-D compliance, it may seem reasonable to assume that all 2-D compliance values for a

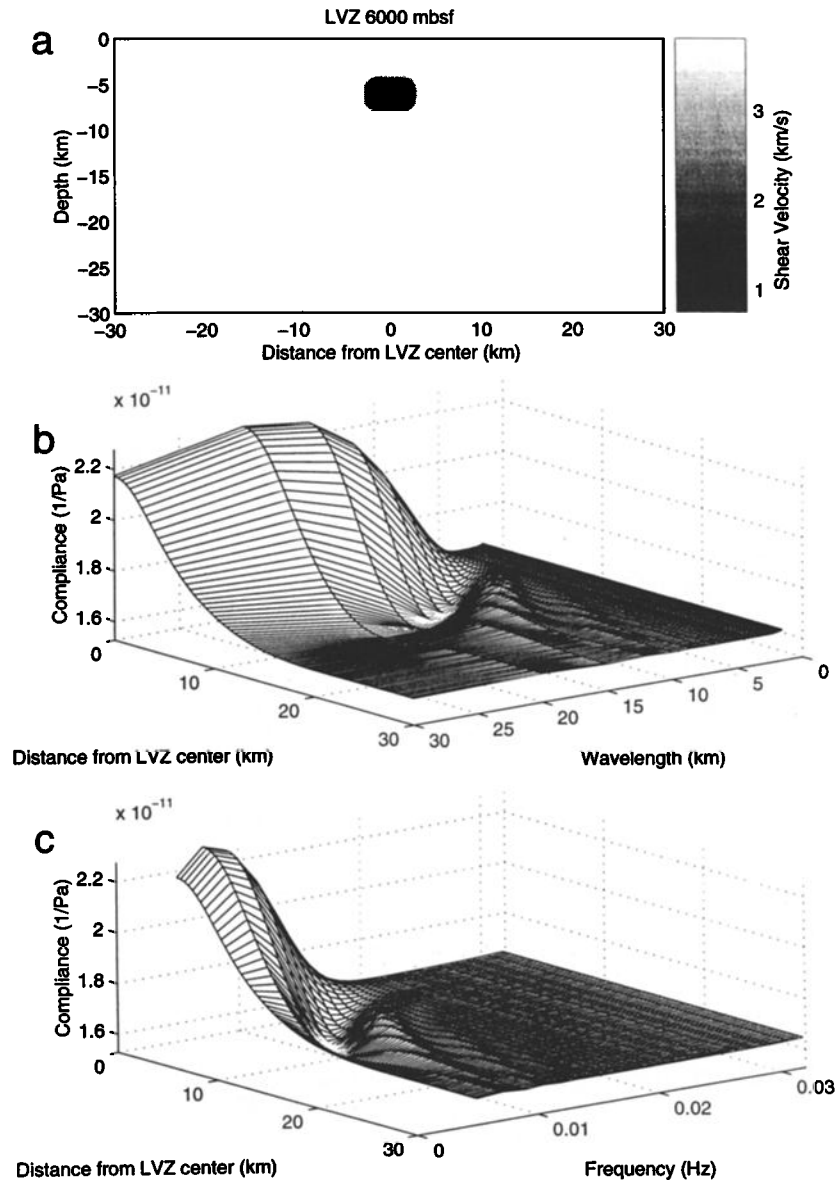


**Figure 10.** LVZ centered 6 km below the seafloor.  $V_P = 4$  km/s,  $V_S = 0.75$  km/s,  $\rho = 2500$  kg/m<sup>3</sup>,  $\mu = 1.4$  GPa in the LVZ, while the surrounding material is uniform gabbroic rock ( $V_P = 7$  km/s,  $V_S = 3.8$  km/s,  $\rho = 3000$  kg/m<sup>3</sup>,  $\mu = 43$  GPa). Because compliance values are symmetric about the origin, compliance values are shown for only one-half the model. (a) Shear velocity. (b) Seafloor compliance as a function of forcing wavelength and horizontal distance from the center of the model. (c) Seafloor compliance as a function of frequency and horizontal distance.

given crustal model should be located within the maximum and minimum bounds of 1-D compliance functions for that model. However, this is not the case. For example, over the 3 km deep LVZ model, compliance values within 1 km of the LVZ are larger than the 1-D values at high frequencies. For the same model, compliance values more than 3 km off axis are lower than the minimum 1-D value at frequencies centered around 0.016 Hz. The overshoot and undershoot of the 1-D compliance bounds are better viewed in Figure 12, which shows compliance as a function of distance across the 3 km deep LVZ model for a 5 km forcing wavelength (equivalent to a cut through Figure 11a at 0.0176 Hz). The overshoot and undershoot are greatest (up to 15% of the on-axis

compliance peak) at forcing ocean surface wavelengths similar to the width of the LVZ (3 km plus 3 km of transition zone). The result of the undershoot is that 1-D modeling at the off-axis sites may suggest higher shear strength at intermediate depths than is appropriate. The overshoot, being located on the high-frequency side of the compliance peak, will suggest even shallower LVZ depths when analyzed using 1-D modeling. The off-axis minimum observed for the 6 km deep LVZ model (Figure 11b) has smaller amplitude than that observed for the 3 km deep model, because the largest compliance signal for the 6 km deep model is concentrated at wavelengths much longer than the LVZ width.

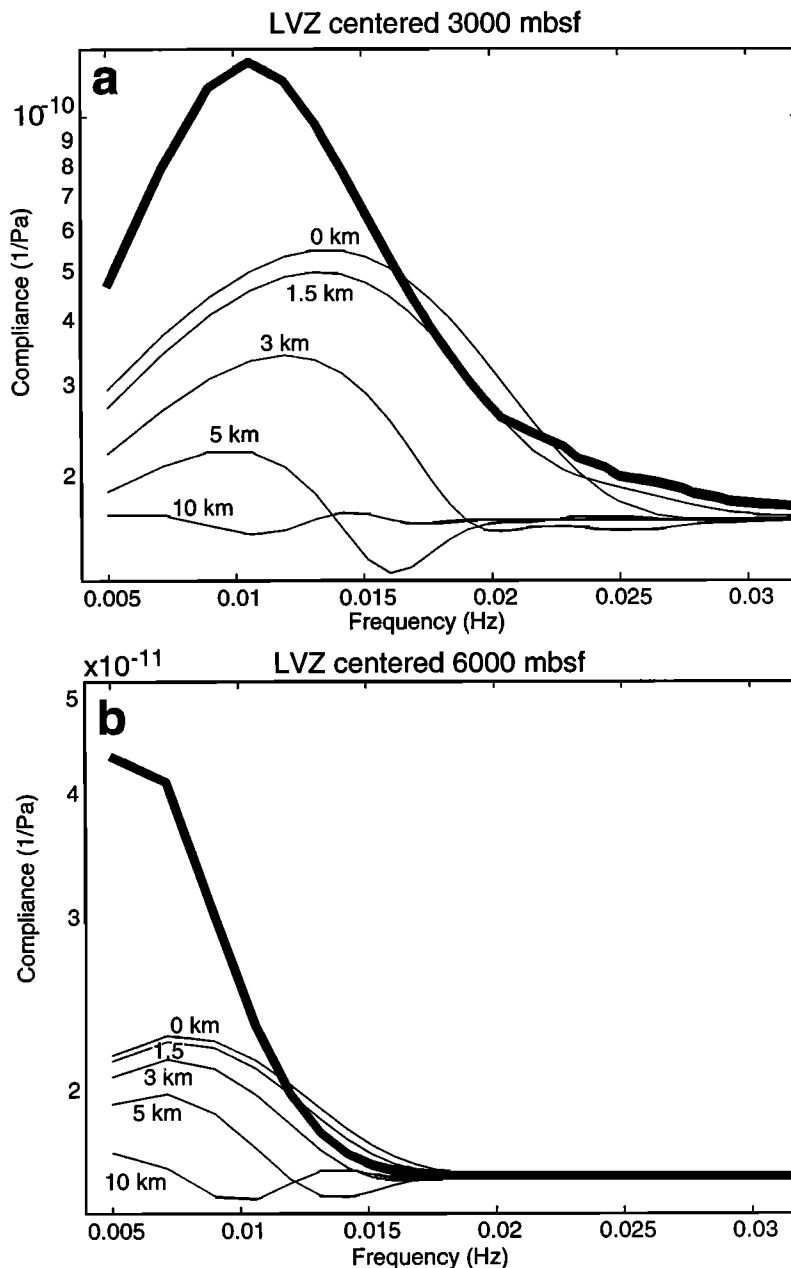


**Figure 11.** Compliance modeled over LVZs: (a) LVZ centered 3 km beneath the seafloor, (b) LVZ centered 6 km beneath the seafloor. Thick line is compliance calculated using a 1-D model of the LVZ. Thin lines are seafloor compliance functions at 0, 1.5, 3, 5, and 10 km horizontally from the LVZ center.

**5.3. East Pacific Rise, 9°N Model**

The final crustal model we evaluate using the 2-D finite difference code is an East Pacific Rise cross section near 9°30'N, based on the expanding spread profiles (ESPs) of Vera et al. [1990], with the melt lens depth and dimensions modified to fit those determined using the seismic reflection modeling of Husenieder et al. [1996]. To accommodate the numerical modeling requirement that all structure is more than 10 model grid elements across, the velocity-depth profiles were filtered to suppress wavelengths shorter than 1.2 km. Only the axial melt lens thickness is significantly modified by this filtering. The LVZ in the filtered on-

axis model actually generates higher 1-D compliance than the LVZ in the original model, because the increase in LVZ thickness overcomes the higher shear velocities within.

A 2-D crustal cross section (Plate 1a) was created from the filtered 1-D models by cubic spline interpolation between the profiles and an assumption of symmetry across the rise axis. The 10 km off-axis profile is extended to all distances greater than 10 km off axis. The compliance function (Plate 1b and 1c) is dominated by two features: (1) high values off axis at high frequencies, and (2) an on-axis compliance peak centered at 0.02 Hz. The rapid increase in high-frequency compliance values off axis is the result of thick-

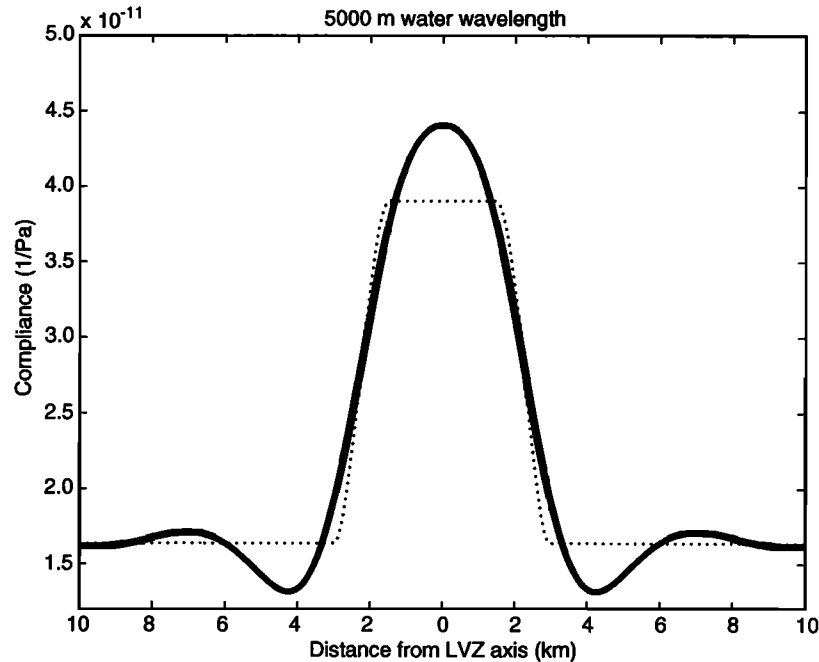


**Figure 12.** Compliance generated by a 5 km wavelength pressure source across the 3 km deep LVZ model. Dotted line is 1-D compliance.

ening of the low-shear-velocity layer 2A. The on-axis compliance peak is generated by the axial LVZ.

The difference between the seafloor compliance function and that predicted using a 1-D approximation is illustrated in Figure 13. Two-dimensional compliance is compared to the 1-D approximation for locations 0, 2.1, 3.1, and 10 km off axis. On axis, the peak in the 2-D compliance function generated by the crustal LVZ is at higher frequency and is smaller than the peak predicted using 1-D compliance modeling. Off axis, a compliance maximum is observed that decreases in amplitude and shifts to lower frequencies with increasing distance off axis. By 10 km off axis this peak generates only a small perturbation at the lowest compliance frequencies.

To demonstrate the effect of 2-D structure on crustal models created using 1-D compliance forward modeling, we calculated 1-D shear velocity models fitting the 2-D compli-

ance data (Figure 14). The models were constructed using a linearized geophysical inverse technique known as Occam's inversion [Constable *et al.*, 1987], providing the smoothest model that fits the data to within data errors. Assuming the oceanic crustal structure varies only with depth, the inversion produces an LVZ only if required by the data. No assumptions about geological structure are used, so the resulting shear velocities are maximally smooth at the expense of deviating from known geological boundaries. This approach allows construction of an unbiased shear velocity model. Once features required by the data are determined, they may be modified to fit geological intuition. Because compliance is most sensitive to low shear velocities, low-shear-velocity zones are the best constrained part of the model. Conversely, regions of high shear strength are less well constrained by the data.

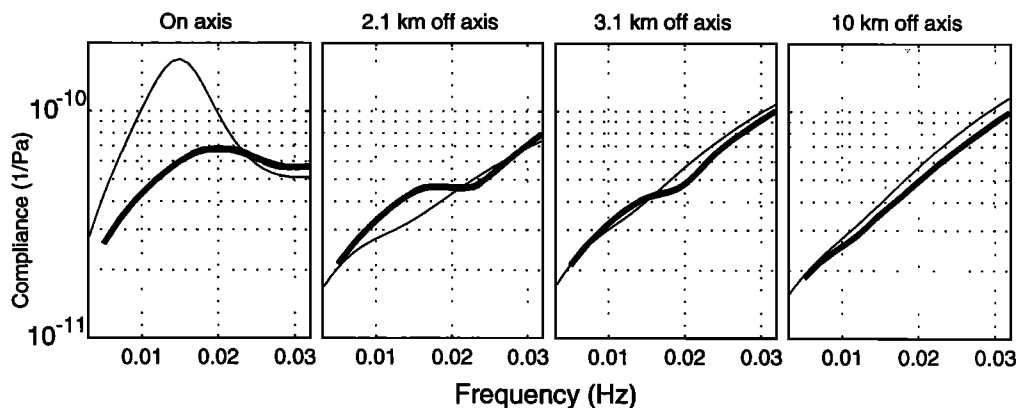


**Figure 13.** One-dimensional compliance calculated for the 9°30'N East Pacific Rise (EPR) model (thin lines) compared to 2-D compliance (thick lines).

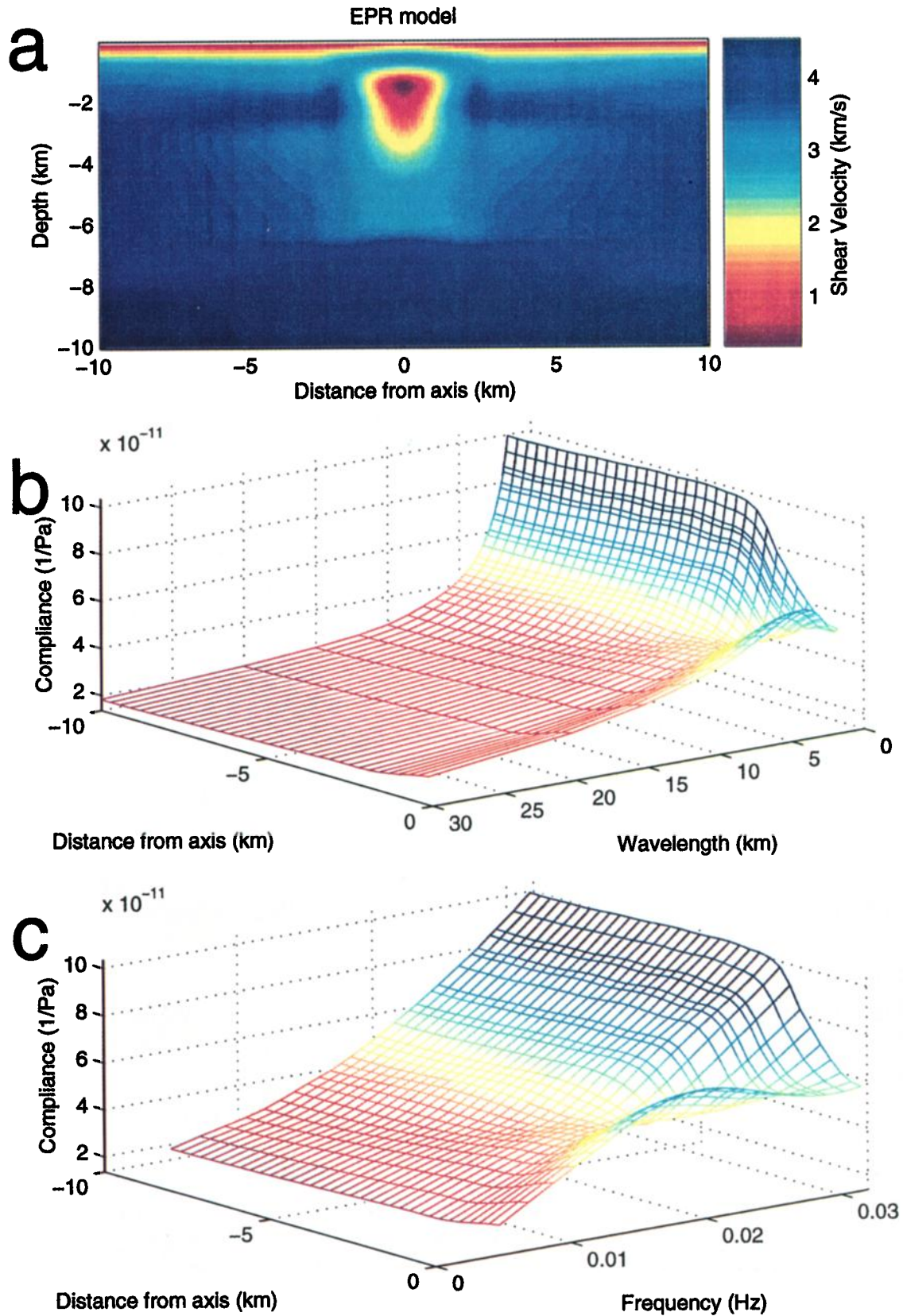


**Plate 1.** Fast spreading mid-oceanic ridge model based on expanding spread profile (ESP) models of *Vera et al.* [1990]. The model is the same size (60 km wide, 30 km deep) as the other 2-D models, but the plots focus within 10 km of the rise axis, where all the changes in the model and in compliance appear. (a) Shear velocity. (b) Seafloor compliance as a function of forcing wavelength and horizontal distance. (c) Seafloor compliance as a function of frequency and horizontal distance.

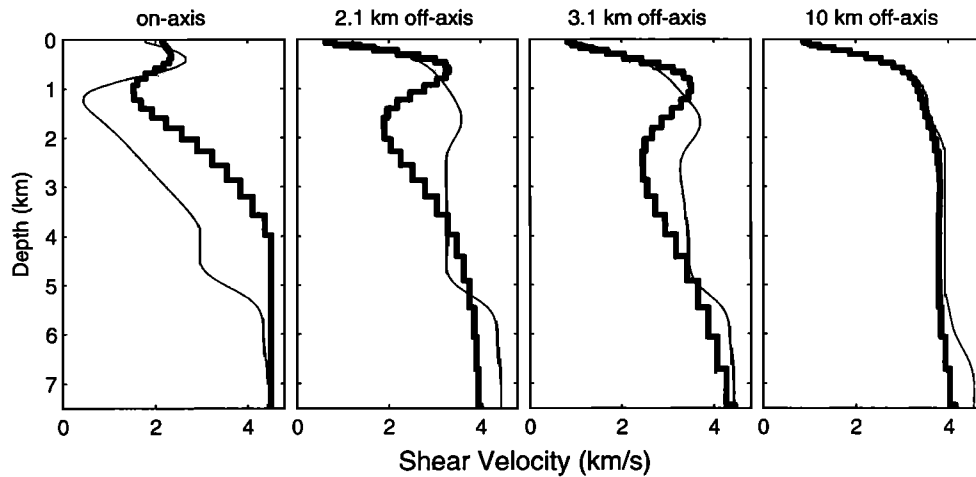


**Figure 14.** Minimum structure 1-D shear velocity models fitting the 2-D compliance data (thick lines), compared with 2-D model shear velocities beneath each measurement site (thin lines). Uncertainties are added to the compliance functions before inverting. The 1-D inversion program required a 3% compliance before it could fit the on-axis data to within the expected error. This is the largest misfit required to fit any of the compliance functions, and is caused by the inability of 1-D compliance to model the rapid decrease in the compliance function at low frequencies due to increased sensitivity of long wavelengths to off-axis structure. The inversion attempts to fit the low-frequency decrease by increasing deep shear velocities to non-physical values. Further off axis, smaller uncertainties were needed to fit the data. A compliance uncertainty of 2% was adequate to fit compliance 2.1 and 3.1 km off axis, and 0.5% uncertainty sufficed for the 10 km off-axis data.

The resulting 1-D shear velocity models (Figure 14) have many of the features of the original crustal structure, but the lateral structure variations introduce predicted differences. On axis, the LVZ is modeled as slightly too shallow and with a minimum shear velocity about 2 times too large. Off axis, the LVZ appears to deepen with distance away from the rise axis. By 10 km off axis, the effect of the axial LVZ is small. The increase in shear velocity at the modeled Moho is not duplicated in the compliance data because it does not correspond to a large enough change in  $1/\mu$  to overcome the limited compliance depth sensitivity.

In Figure 14, beneath the 2.1 and 3.1 km off-axis sites, modeled shear velocities are too high at approximately 0.7 km depth. This overestimate of shear velocities is common where a high-velocity region is sandwiched between two low-velocity regions. The compliance data require a high-velocity region between layer 2A and the LVZ, but compliance is least sensitive to shear velocity errors in high-velocity regions. Therefore, the inversion here allows too high shear velocities in order to obtain a smoother profile.

While the 1-D inversions give a distorted representation of the original crustal structure, they are still useful in that the LVZ was detected and placed within 20% of the correct depth. More importantly, no spurious LVZs were inferred. As the 1-D compliance modeling and inversion is significantly more computationally efficient than 2-D modeling, the 1-D inversions provide a useful first step to interpreting crustal structure from compliance data.

## 6. Modeling Small Crustal Features

Because of computer memory limitations, the finite difference code can not yet model compliance over small crustal

features such as the 10–80 m tall East Pacific Rise (EPR) melt lens [Kent *et al.*, 1993], or the rapid variations in layer 2A thickness near the EPR axis [Harding *et al.*, 1993]. Where features like these may exist within the crust, but are not constrained by existing geophysical data, the finite difference code can be used to construct a minimum structure (smoothed) shear velocity model from compliance data. Where the size of small crustal features is well constrained, crustal shear velocities are better estimated using a 2-D compliance approximation that we describe below.

The minimum structure model is the smoothest model in some sense that fits the compliance data. In the absence of prior structural constraints, minimizing the model structure maximizes the probability that features in the model are required by the data [Constable *et al.*, 1987]. Minimum structure models constructed from compliance data smooth crustal features smaller than the ocean depth, so a thin crustal melt lens will be modeled as a more diffuse low-velocity zone. Because of this smoothing, minimum structure models can be constructed using the finite difference code. The models are useful because they reveal low-velocity zones and indicate the minimum required shear velocity anomaly.

Where the crustal structure is already known, crustal shear velocities are better estimated by combining the compliance data with the structural constraints. We work toward a complete modeling code that will handle very small scale structure. For now, if crustal structure varies too rapidly to model using the finite difference code, shear velocities can be estimated using a “2-D approximation” based on the 1-D compliance code.

The 2-D approximation is generated by spatial low-pass filtering of compliance calculated using the 1-D approximation. The 1-D compliance code can model rapid vertical ve-

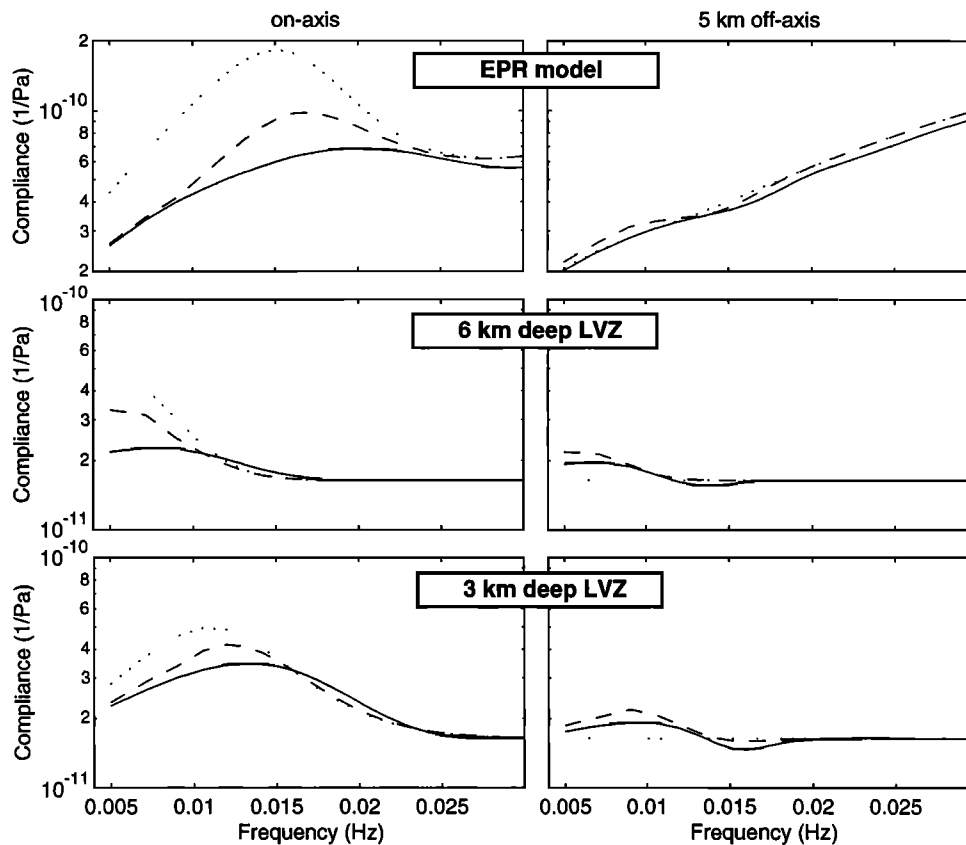


**Figure 15.** A comparison of seafloor compliance calculated for the 2-D models in this paper using the finite difference code (solid line), the 1-D approximation (dotted line), and the 2-D approximation (dashed line). The 2-D approximation is created by spatially low-pass filtering the 1-D approximation with a cutoff wavelength tied to the wavelength of the forcing ocean waves. The 2-D approximation significantly improves compliance modeling compared to the 1-D approximation, with little additional computational cost.

locity variations, and the spatial filtering approximates the effect of lateral shear velocity variations. The cutoff wavelength is the shorter of (1) the forcing ocean wave wavelength, and (2) the structural wavelength of the crust. The structural wavelength is empirically determined and depends on the crustal rigidity: The shortest structural wavelength for the models in this paper is 15 km. Figure 15 compares compliances calculated for the EPR and LVZ models using the 2-D approximation (with structural wavelength equal to 15 km), the 1-D approximation, and the finite difference code. The 2-D approximation is always closer to the true compliance value than is the 1-D approximation. The 2-D approximation overestimates compliance over an LVZ, so shear velocities estimated within the LVZ will be upper bounds.

## 7. Discussion

The goal of the 2-D seafloor compliance modeling presented in this paper is to determine if laterally varying crustal structure can be determined from compliance measurements. Two questions examined to this end are (1) does a peak in the compliance function require a crustal LVZ, and (2) does the compliance function respond predictably to changes in crustal structure? Our modeling indicates that a peak in the

compliance function does require a crustal LVZ. This LVZ may, however, be located to the side of the measurement site. If there are no prior constraints on the LVZ location, a series of compliance measurements are required to constrain the LVZ location and shear velocities.

Construction of a new crustal model based on measured seafloor compliance requires that the compliance function responds predictably to changes in crustal structure. The 2-D compliance functions calculated in this paper are indeed predictable. As with one-dimensional compliance, a high compliance amplitude indicates a low crustal shear velocity, and the frequency at which features in the compliance function appear corresponds to the depth of shear velocity variations. We suggest that the best way to generate a crustal model from compliance data is to use the greater speed of the 1-D compliance inversion method, and then to fine-tune the model based on compliance calculated using the 2-D finite difference code. One-dimensional crustal models constructed from each of a series of compliance measurements do not reproduce all the features of a finite width LVZ, but neither do they generate extraneous crustal structure. The 1-D code requires approximately 2 minutes on a desktop workstation to calculate compliance functions at every surface element of a 300x600 element model, compared to 3-1/2 hours

of Cray C90 supercomputer time required to run the 2-D finite difference code for the same model.

The finite difference modeling in this paper is limited to seafloor compliance generated by ocean surface waves traveling perpendicular to 2-D crustal structure. We have not modeled compliance over three-dimensional (3-D) structures because the resolution would be too coarse (with current computational memory limits). No new physics is introduced by extending the modeling to three dimensions, so that the effect of 3-D structure on compliance should not be qualitatively different than the effect of 2-D structure. Construction of crustal models based on compliance values is, however, limited to the 2-D models for which compliance can currently be calculated. Mid-ocean ridges and linear faults generally exhibit much greater variability across strike than along strike, making them logical choices for 2-D compliance modeling. The assumption of 2-D structure can be tested by measuring seafloor compliance along strike.

## 8. Conclusions

Seafloor compliance measurements provide valuable constraints on the role of fluids in the accretion and alteration of oceanic crust and sediments, because the compliance function is especially sensitive to regions of low shear velocity. Compliance measurements are particularly useful at oceanic spreading centers, where the quantity, location, and role of crustal and upper mantle melt are still debated [e.g., *Phipps Morgan and Chen, 1993; Boudier and Nicolas, 1996; Husse-noeder et al., 1996; Kelemen, 1997*]. Seafloor compliance measurements on the intermediate spreading Juan de Fuca Ridge, and on the fast spreading East Pacific Rise at 9°N [*Crawford et al., 1995*] detect low-velocity zones associated with crustal melt. The mid-crustal melt lens at 9°N on the East Pacific Rise had previously been imaged using active seismic methods, but the sensitivity of the compliance measurement to shear velocities throughout the crust improves constraints on the melt supply beneath the lens. The narrow width of the shallow melt lens and underlying partial melt zone is associated with compliance values that change rapidly away from the spreading axis. Interpretation of the data must take into account the effect on compliance of lateral variations in crustal structure.

In this paper, compliance functions were calculated for 1-D and 2-D oceanic crustal models to determine compliance sensitivity to the intensity, depth, and width of crustal shear velocity anomalies. Seafloor compliance is, to first approximation, inversely proportional to the shear modulus in the oceanic crust. For comparison with results of active seismic studies, the shear velocity ( $V_S$ ) is often inferred from the shear modulus and models of crustal density. Over low-shear-strength regions such as crustal melt and partial melt zones, porous crust, and sediments, compliance values are determined by the  $V_S$  structure. With increasing shear strength, the compliance function becomes more dependent on compressional velocity ( $V_P$ ), and is equally dependent on  $V_P$  and  $V_S$  for a Poisson solid.

Low-velocity zones generate a peak in the compliance function over a limited frequency band. For 1-D crustal models, the frequency of the maximum compliance value corresponds to ocean surface wavelengths ranging from 4 to 6 times the LVZ depth, dependent on the LVZ intensity. The longest wavelength providing useful compliance data, and therefore the maximum depth of compliance sensitivity, increases with increasing water depth. For seafloor depths greater than 2 km, compliance values are sensitive to crustal structure to 6 km depth or more.

The seafloor compliance function spatially smooths lateral variations in crustal structure over a scale approximately equivalent to one-half of the wavelength of the ocean surface gravity waves causing the seafloor deformation. As a result, the compliance function over a finite width low-velocity zone has a peak with lower amplitude and whose center frequency is higher (shorter wavelength) than is predicted by 1-D modeling. To the side of the low-velocity zone, the compliance amplitude decreases most rapidly at high frequencies, shifting the compliance maximum to lower frequencies. Seafloor models constructed over a finite width LVZ using only 1-D modeling will therefore overestimate both the depth of and the shear velocity within the LVZ, and will show an apparent deepening of the LVZ to the sides. There is no indication that shear velocity profiles created using 1-D modeling add extraneous structure, and so these profiles are a good starting point for construction of crustal models. The 2-D finite difference code can refine these crustal models.

The 2-D modeling demonstrates that a series of compliance measurements are needed to constrain the location and dimensions of a crustal LVZ. The rate of change in amplitude and frequency of the compliance function, away from the compliance maximum associated with an LVZ, provides essential constraints on the LVZ shear velocity and width. The compliance modeling performed here indicates that observed compliance changes over a few kilometers or less at mid-ocean ridges and at faults are caused by rapid lateral variations in crustal shear velocity. The seafloor compliance data can be used to better constrain the shear velocity structure of, and therefore the melt distribution and porosity within, the oceanic crust.

## Appendix: Forward Modeling of Seafloor Compliance Using Centered Finite Differences

Let  $x$  and  $z$  be the horizontal and vertical rectangular coordinates in a two-dimensional medium, and let the  $z$  axis be positive upward. Two equations describe Newton's second law for motion in the plane of the model:

$$\begin{aligned}\rho \frac{\partial^2 u}{\partial t^2} &= \frac{\partial \tau_{xx}}{\partial x} + \frac{\partial \tau_{xz}}{\partial z} \\ \rho \frac{\partial^2 w}{\partial t^2} &= \frac{\partial \tau_{zz}}{\partial z} + \frac{\partial \tau_{xz}}{\partial x}\end{aligned}\tag{A1}$$

where  $u$  and  $w$  are horizontal displacements,  $\rho$  is the density, and  $t$  is time [*Aki and Richards, 1980*]. The traction terms  $\tau_{ij}$  are defined as

$$\begin{aligned}
\tau_{xz} = \tau_{zx} &\equiv \mu \left( \frac{\partial u}{\partial z} + \frac{\partial w}{\partial x} \right) \\
\tau_{xx} &\equiv (\lambda + 2\mu) \frac{\partial u}{\partial x} + \lambda \frac{\partial w}{\partial z} \\
\tau_{zz} &\equiv (\lambda + 2\mu) \frac{\partial w}{\partial z} + \lambda \frac{\partial u}{\partial x}.
\end{aligned} \quad (\text{A2})$$

We assume the forcing function is harmonic, so that

$$\frac{\partial^2 u}{\partial t^2} = -\omega^2 u, \quad \frac{\partial^2 w}{\partial t^2} = -\omega^2 w. \quad (\text{A3})$$

Combining (A1), (A2), and (A3) gives

$$\begin{aligned}
-\omega^2 \rho u &= \frac{\partial(\lambda + 2\mu)}{\partial x} \frac{\partial u}{\partial x} + \frac{\partial \mu}{\partial z} \frac{\partial u}{\partial z} \\
&+ (\lambda + 2\mu) \frac{\partial^2 u}{\partial x^2} + \mu \frac{\partial^2 u}{\partial z^2} \\
&+ \frac{\partial \mu}{\partial z} \frac{\partial w}{\partial x} + \frac{\partial \lambda}{\partial x} \frac{\partial w}{\partial z} \\
&+ (\lambda + \mu) \frac{\partial^2 w}{\partial x \partial z}
\end{aligned} \quad (\text{A4a})$$

$$\begin{aligned}
-\omega^2 \rho w &= \frac{\partial(\lambda + 2\mu)}{\partial z} \frac{\partial w}{\partial z} + \frac{\partial \mu}{\partial x} \frac{\partial w}{\partial x} \\
&+ (\lambda + 2\mu) \frac{\partial^2 w}{\partial z^2} + \mu \frac{\partial^2 w}{\partial x^2} \\
&+ \frac{\partial \mu}{\partial x} \frac{\partial u}{\partial z} + \frac{\partial \lambda}{\partial z} \frac{\partial u}{\partial x} \\
&+ (\lambda + \mu) \frac{\partial^2 u}{\partial x \partial z}
\end{aligned} \quad (\text{A4b})$$

The boundary conditions are that  $u, w \rightarrow \infty$  as  $z \rightarrow \infty$ , that there is free slip at the interface between the ocean and seafloor, and that pressure at the seafloor takes the form of a plane wave.

We approximate these equations using centered finite differences on a gridded model with constant grid spacing. For an  $M$  row by  $N$  column seafloor model, we construct a finite difference matrix with  $2(M+1)N$  columns corresponding to a  $u$  and  $w$  term for every element of the model matrix plus a “ghost” layer (model row 0) above the model. The first  $2N$  rows of the finite difference matrix contain finite difference equations for the seafloor boundary conditions of free slip

$$w(1, j+1) - w(1, j-1) + u(2, j) - u(0, j) = 0 \quad (\text{A5})$$

and plane wave forcing

$$\begin{aligned}
\lambda [u(1, j+1) - u(1, j-1)] \\
+ (\lambda + 2\mu) [w(0, j) - w(2, j)] = P(x)
\end{aligned} \quad (\text{A6})$$

where  $P(x)$  is a sinusoid of amplitude 1 with integral number of wavelengths across the model that represents pressure at the seafloor. The equations assume the grid spacing  $h$  is equivalent horizontally and vertically. Rows  $2N+1$  to  $2(M+1)N$  contain the centered finite difference equations corresponding to (A4),

$$\begin{aligned}
0 &= 2(\omega^2 \rho h^2 - 2\lambda - 6\mu) u(i, j) \\
&+ \left( 2(\lambda + 2\mu) - h \frac{\partial(\lambda + 2\mu)}{\partial x} \right) u(i, j-1) \\
&+ \left( 2(\lambda + 2\mu) + h \frac{\partial(\lambda + 2\mu)}{\partial x} \right) u(i, j+1) \\
&+ \left( 2\mu + h \frac{\partial \mu}{\partial z} \right) u(i-1, j) \\
&+ \left( 2\mu - h \frac{\partial \mu}{\partial z} \right) u(i+1, j) \\
&+ h \frac{\partial \mu}{\partial z} [w(i, j+1) - w(i, j-1)] \\
&+ h \frac{\partial \lambda}{\partial x} [w(i-1, j) - w(i+1, j)] \\
&+ \frac{\lambda + \mu}{2} [w(i-1, j+1) + w(i+1, j-1) \\
&\quad - w(i-1, j-1) - w(i+1, j+1)]
\end{aligned} \quad (\text{A7a})$$

$$\begin{aligned}
0 &= 2(\omega^2 \rho h^2 - 2\lambda - 6\mu) w(i, j) \\
&+ \left( 2(\lambda + 2\mu) + h \frac{\partial(\lambda + 2\mu)}{\partial z} \right) w(i-1, j) \\
&+ \left( 2(\lambda + 2\mu) - h \frac{\partial(\lambda + 2\mu)}{\partial z} \right) w(i+1, j) \\
&+ \left( 2\mu + h \frac{\partial \mu}{\partial x} \right) w(i, j+1) \\
&+ \left( 2\mu - h \frac{\partial \mu}{\partial x} \right) w(i, j-1) \\
&+ h \frac{\partial \lambda}{\partial z} [u(i, j+1) - u(i, j-1)] \\
&+ h \frac{\partial \mu}{\partial x} [u(i-1, j) - u(i+1, j)] \\
&+ \frac{\lambda + \mu}{2} [u(i-1, j+1) + u(i+1, j-1) \\
&\quad - u(i-1, j-1) - u(i+1, j+1)]
\end{aligned} \quad (\text{A7b})$$

The derivatives of  $\lambda$  and  $\mu$  are calculated using centered finite differences except at the top and bottom of the model, where forward and reverse differences are used. A periodic  $x$  boundary is created by substituting  $u(1, j)$  for  $u(N+1, j)$ ,  $w(1, j)$  for  $w(N+1, j)$ ,  $u(N, j)$  for  $u(0, j)$ , and  $w(N, j)$  for  $w(0, j)$  in these equations. The condition  $u, w \rightarrow 0$  as  $z \rightarrow \infty$  is approximated by zero motion at the bottom of the model. The finite difference equations for row  $M$  do not have a  $w(n, m+1)$  or  $u(n, m+1)$  term, which is equivalent to setting these values to zero.

The finite difference matrix is constructed to maximize its “bandedness”. Columns alternate between  $u$  and  $w$  values, and rows alternate between first the free slip and forcing wave equations and then the  $u$ - and  $w$ -based equations of motion. The solution matrix is  $(2(M+1)N) \times 2S$ , where  $S$  is the number of forcing waves to solve for at once. In general,  $S = 1$  because the forcing wave is tied to the frequency. For seafloor compliance, however, the frequency term  $\omega$  in (A7) is insignificant because  $\omega^2 \rho h^2 \ll 2\lambda + 6\mu$  for frequency  $f < 0.05$  Hz and grid spacing  $h \leq$

125 m. Test runs with and without the inertial terms are indistinguishable. Therefore, all pressure modes can be placed as double-columned entries into the solution array. Odd columns contain  $\sin(k_N j h)$ , and even columns contain  $\cos(k_N j h)$ , where

$$k_N \equiv \frac{2\pi N}{W}$$

and  $W$  is the model width.

Simultaneous solution of the finite difference equations requires a substantial amount of memory. A  $2NM \times 2NM$  finite difference array is needed to solve an  $N \times M$  model. The matrix is sparse and requires a maximum of 20 nonzero entries per row. The memory requirements are reduced by converting the finite difference matrix into a  $8N \times 2NM$  band matrix. A  $300 \times 600$  model matrix generates a double precision  $1.73 \times 10^9$  element band matrix requiring 12.8 Gigabytes of memory. We use a commercial virtual memory mathematical library on a Cray C90 supercomputer at the San Diego Supercomputer Center to solve matrices up to 16 Gigabytes. The  $300 \times 600$  model requires 82 minutes of C90 CPU time to solve.

**Acknowledgments.** We thank the San Diego Supercomputer Center and the Scripps Institution of Oceanography block grant for use of the Cray C90 supercomputer. Research support was provided by ONR grant N00014-95-1-0054 and the ONR MPL/ARL Program; we thank Joseph Kravitz for his support. We thank Glen Lerley for numerous discussions regarding the finite difference numerical code, and Harold Seigel for his suggestion that the gravitational attraction of ocean surface waves might be significant in the seafloor acceleration signal. Gail Christeson and an anonymous reviewer provided constructive and thoughtful reviews of the original manuscript.

## References

- Aki, K., and P.G. Richards, *Quantitative Seismology: Theory and Methods*, 932 pp., W. H. Freeman, San Francisco, Calif., 1980.
- Boudier, F., and A. Nicolas, Magma chambers in the Oman ophiolite; fed from the top and bottom, *Earth Planet. Sci. Lett.*, **144**, 239–250, 1996.
- Carlson, R.L., and G.S. Raskin, Density of the ocean crust, *Nature*, **311**, 555–558, 1984.
- Christensen, N.I., and M.H. Salisbury, Sea floor spreading, progressive alteration of layer 2 basalts, and associated changes in seismic velocities, *Earth Planet. Sci. Lett.*, **15**, 367–375, 1972.
- Christensen, N.I., Ophiolites, seismic velocities and oceanic crustal structure, *Tectonophysics*, **47**, 131–157, 1978.
- Christeson, G.L., G.M. Purdy, and K.M.M. Rohr, Structure of the Northern Symmetrical segment of the Juan de Fuca Ridge, *Mar. Geophys. Res.*, **15**, 219–240, 1993.
- Constable, S.C., R.L. Parker, and C.G. Constable, Occam's inversion: A practical algorithm for generating smooth models from electromagnetic sounding data, *Geophysics*, **52**, 289–300, 1987.
- Cox, C.S., T. Deaton, and S.C. Webb, A deep sea differential pressure gauge, *J. Atmos. Oceanic Technol.*, **1**, 237–246, 1984.
- Crawford, W.C., Determination of oceanic crustal shear velocity structure from seafloor compliance measurements, Ph.D. thesis, Univ. of Calif., San Diego, La Jolla, 1994.
- Crawford, W.C., S.C. Webb, and J.A. Hildebrand, Seafloor compliance observed by long-period pressure and displacement measurements, *J. Geophys. Res.*, **96**, 16151–16160, 1991.
- Crawford, W.C., S.C. Webb, and J.A. Hildebrand, The Coaxial segment crustal magma source, *Eos Trans. AGU*, **75**(44), Fall Meet. Suppl., 617, 1994.
- Crawford, W.C., S.C. Webb, and J.A. Hildebrand, Low shear velocity zones within the East Pacific Rise at 9 degrees, 48' N, *Eos Trans. AGU*, **76** (46), Fall Meet. Suppl., 401, 1995.
- Cudrak, C.F., and R.M. Clowes, Crustal structure of Endeavour Ridge segment, Juan de Fuca Ridge, from a detailed seismic refraction survey, *J. Geophys. Res.*, **98**, 6329–6349, 1993.
- Fischer, P.J., and G.I. Mills, The offshore Newport-Inglewood-Rose Canyon fault zone, California; structure, segmentation and tectonics, in *Environmental Perils: San Diego Region*, edited by P.L. Abbott, and W.J. Elliott, pp. 17–36, San Diego Assoc. Geol., San Diego, Calif., 1991.
- Gill, A.E., *Atmosphere-Ocean Dynamics*, 662 pp., Academic, San Diego, Calif., 1982.
- Gomberg, J.S., and T.G. Masters, Waveform modeling using locked-mode synthetic and differential seismograms: Application to determination of the structure of Mexico, *Geophys. J.*, **94**, 193–218, 1988.
- Harding, A.J., G.M. Kent, and J.A. Orcutt, A multichannel seismic investigation of upper crustal structure at 9 degrees N on the East Pacific Rise: implications for crustal accretion, *J. Geophys. Res.*, **98**, 13925–13944, 1993.
- Horen, H., M. Zamora, and G. Dubuisson, Seismic waves velocities and anisotropy in serpentinized peridotites from Xigaze ophiolite; abundance of serpentine in slow spreading ridge, *Geophys. Res. Lett.*, **23**(1), 9–12, 1996.
- Husenoeder, S.A., J.A. Collins, G.M. Kent, R.S. Detrick, A.J. Harding, J.A. Orcutt, J.C. Mutter, and P. Buhl, Seismic analysis of the axial magma chamber reflector along the southern East Pacific Rise from conventional reflection profiling, *J. Geophys. Res.*, **101**, 22087–22105, 1996.
- Kelemen, P.B., Geochemistry of gabbro sills in the crust-mantle transition zone of the Oman ophiolite; implications for the origin of the oceanic lower crust, *Earth Planet. Sci. Lett.*, **146**, 475–488, 1997.
- Kent, G.M., A.J. Harding, and J.A. Orcutt, Distribution of magma beneath the East Pacific Rise between the clipperton transform and the 9 degrees 17' N deval from forward modeling of common depth point data, *J. Geophys. Res.*, **98**, 13945–13969, 1993.
- Lacoste, L.J.B., Measurement of gravity at sea and in the air, *Rev. Geophys.*, **5**, 477–526, 1967.
- Murase, T., and H. Fukuyama, Structure and properties of liquids and glasses, *Year Book, Carnegie Inst. Washington*, **79**, 307–310, 1980.
- Phipps Morgan, J., and Y.J. Chen, The genesis of oceanic crust: Magma injection, hydrothermal circulation, and crustal flow, *J. Geophys. Res.*, **98**, 6283–6297, 1993.
- Sorrels, G.G., and T.T. Goforth, Low frequency earth motion generated by slowly propagating, partially organized pressure fields, *Bull. Seismol. Soc. Am.*, **63**, 1583–1601, 1973.
- Spudich, P., and J. Orcutt, A new look at the seismic velocity structure of the oceanic crust, *Rev. Geophys.*, **18**(3), 627–645, 1980.
- Teng, L.S., and D.S. Gorsline, Late Cenozoic sedimentation in California Continental Borderland basins as revealed by seismic facies analysis, *Geol. Soc. Am. Bull.*, **101**, 27–41, 1989.
- Torii, T., Determination of shear modulus profile by inverse analysis of wave-induced bottom motion, master's thesis, Univ. of Miami, Coral Gables, Fla., 1985.
- Trevorrow, M.V., and T. Yamamoto, Summary of marine sedimentary shear modulus and acoustic speed profile results using a gravity wave inversion technique, *J. Acoust. Soc. Am.*, **90**(1), 441–456, 1991.
- Trevorrow, M.V., T. Yamamoto, M. Badiey, A. Turgut, and C. Conner, Experimental verification of sea-bed shear modulus profile inversions using surface gravity (water) wave-induced sea-bed motion, *Geophys. J.*, **93**, 419–436, 1988.
- Vera, E.E., J.C. Mutter, P. Buhl, J.A. Orcutt, A.J. Harding, M.E. Kappus, R.S. Detrick, and T.M. Brocher, The structure of 0- to 0.2 m.y.-old oceanic crust at 9°N on the East Pacific Rise from

expanding spread profiles, *J. Geophys. Res.*, *95*, 15529–15556, 1990.

Yamamoto, T., and T. Torii, Seabed shear modulus profile inversion using surface gravity (water) wave-induced bottom motion, *Geophys. J. R. Astron. Soc.*, *85*, 413–431, 1986.

Yamamoto, T., M.V. Trevorrow, M. Badiy, and A. Turgut, Determination of the seabed porosity and shear modulus profiles using a gravity wave inversion, *Geophys. J. Int.*, *98*(1), 173–182, 1989.

---

W. C. Crawford, J. A. Hildebrand, and S. C. Webb, Marine Physical Laboratory, Scripps Institution of Oceanography, 9500 Gilman Drive, La Jolla, CA 92093-0205. (e-mail: wrcrawford@ucsd.edu; jahildebrand@ucsd.edu, swebb@ucsd.edu)

(Received June 16, 1997; revised November 12, 1997; accepted November 25, 1997.)